ISCTE ⬡ IUL

Instituto Universitário de Lisboa

DEPARTMENT OF COMPUTER SCIENCE AND TECHNOLOGY

On the Performance of M-QAM optical signals in ROADM based Optical Networks

Dissertation presented in partial fulfillment of the requirements for the

Masters Degree on Telecommunications and Computer Science

by

Hélio Ferreira Paulo Simeão

Supervisors:

Dr. Luís Cancela, Assistant Professor,

ISCTE-IUL

Dr. João Rebola, Assistant Professor,

ISCTE-IUL

June, 2016

Acknowledgements

I am thankful for having as supervisors in this dissertation, Prof. Luís Cancela and Prof. João Rebola. This journey would not have been possible to complete without their continuous support and guidance, especially after times where I wasn't as present as I should be. I would also like to thank Instituto de Telecomunicações (IT), for the work conditions in their facilities.

Special thanks to my colleague Bruno Pinheiro, for his help in the development of the MC simulator.

Lastly, I know I could never have reached this academic milestone without my friends and family.

Thank you all.

Resumo

As limitações do nivel físico das redes ópticas, nomeadamente a diafonia (*crosstalk*) devido ao isolamento imperfeito de elementos de redes de fibra óptica, como os Multiplexadores Ópticos de Adição/Extracção Reconfiguráveis (ROADMs), podem constituir um factor limitativo no desempenho das redes ópticas.

Nesta dissertação, foi estudado através de simulação de Monte-Carlo (MC), o impacto do *crosstalk* homódino devido a sinais interferentes com o formato de modulação em amplitude e em quadratura (M-QAM), no desempenho dos receptores coerentes de sinais 4-QAM e 16-QAM. Foram também estudados vários Selectores de Comprimento de Onda (WSS), um componente dos ROADMs, e em que cada WSS tem um filtro óptico com um perfil diferente.

Duas métricas de *crosstalk*, *unweighted crosstalk* e *weighted crosstalk*, foram usadas para estudar a degradação do desempenho do sistema de comunicações ópticas referente à relação de sinal-ruído óptica (OSNR), no receptor coerente. A diferença entre estas duas métricas, é o facto de o *weighted crosstalk* levar em consideração que o conteúdo espectral perto do centro da largura de banda do canal, tem um impacto maior do que o conteúdo espectral perto das margens da largura de banda do canal. Analisando os resultados com a métrica *unweighted crosstalk*, foi possível concluir que WSSs com filtros ópticos com a banda de rejeição maior e mais centrada com a largura de banda do canal, obtiveram melhor desempenho em relação à penalidade de OSNR medida no receptor coerente. Usando o *weighted crosstalk* como métrica, foi observado que todos os WSSs registaram desempenhos semelhantes em termos de penalidade de OSNR. Podemos concluir, que o *weighted crosstalk* constitui uma métrica bastante fiável a prever desempenhos de sistemas de comunicações ópticos, independentemente do perfil dos filtros usados em cada WSS.

Palavras-chave: Crosstalk homódino, simulação de Monte-Carlo, Multiplexadores Ópticos de Adição/Extracção Reconfiguráveis, weighted crosstalk

Abstract

The optical network physical layer limitations, in particular, the crosstalk due to imperfect isolation of optical network switching components, such as Reconfigurable Optical Add/Drop Multiplexers (ROADMs), can become a limiting factor in the performance of these networks.

In this work, the impact of in-band crosstalk due to M-ary quadrature amplitude modulation (M-QAM) interferers on the performance of 4-QAM and 16-QAM coherent receivers in ROADM based networks is analysed, using Monte Carlo (MC) simulation. Several Wavelength Select Switch (WSS) models, a ROADM component, were studied, and each WSS model had a different optical filter profile.

Two crosstalk metrics, unweighted crosstalk and weighted crosstalk, are used to measure the system performance degradation regarding the Optical Signal-to-Noise Ratio (OSNR) penalty at the coherent receiver. The difference between the two, is the fact that weighted crosstalk takes into account that the spectrum content closer to the center of the channel bandwidth has more impact than spectral content closer to the edges of the channel bandwidth. Using unweighted crosstalk metric, it can be concluded that optical filters with a wider rejection bandwidth in the center of the channel, have a better performance in terms of OSNR penalty at the coherent receiver. With the weighted crosstalk metric, it was observed that regardless of the WSS filter profile, the OSNR penalty performances of each WSS were similar. It can be concluded that the weighted crosstalk metric is very reliable at predicting system performances independently of the filter shape present in the WSS.

Keywords: In-band crosstalk, Monte Carlo simulation, reconfigurable optical add/drop multiplexer, weighted crosstalk

Contents

List of Figures

List of Tables

List of Acronyms

ASE   Amplified Spontaneous Emission

AWGN   Additive White Gaussian Noise

BEP   Bit-Error Probability

BER   Bit Error Rate

DPSK   Differencial Phase-Shift Keying

DQPSK   Differential Quadrature Phase-Shift Keying

DSP   Digital Signal Processing

EDFA   Erbium-Doped Fiber Amplifier

DFT   Discrete Fourier Transform

DWDM   Dense Wavelength-Division Multiplexing

FFT   Fourier Fast Transform

IFFT   Inverse Fourier Fast Transform

IP   Internet Protocol

ISI   Intersymbolic Interference

LO   Local Oscillator

MC   Monte Carlo

M-PSK   M-ary Phase-Shift Keying

M-QAM   M-ary Quadrature Amplitude Modulation

OOK   On-Off Keying

OPM   Optical Power Monitor

OSA   Optical Spectrum Analyzer

OSNR   Optical Signal-to-Noise Ratio

PBS   Polarization Beam Spliter

PDF   Probability Density Function

PDM   Polarization Division Multiplexing

PSD   Power Spectral Density

ROADM Reconfigurable Optical Add-Drop Multiplexer

SNR   Signal-to-Noise Ratio

WSS   Wavelength Selective Switch

List of Symbols

Δf Frequency resolution

λ_0 Selected signal wavelength

λ_{XT} Crosstalk signal wavelength

$\mathfrak{F}$ Fourier Transform

ν_0 Optical carrier frequency

ν_{LO} Local oscillator optical frequency

$\Phi(t)$ Signal phase

B_{OSA} Optical Spectrum Analyzer bandwidth

B_{sim} Simulation bandwidth

$E[.]$ Expected value

E_0 Optical field of the selected signal

E_{LO} Local oscillator electrical field

h Planck constant

N_0 ASE noise power spectrum density

N_a Number of samples per symbol

N_{ASE} ASE noise power spectrum density

N_e Number of erroneous bits

N_I ASE noise power spectrum density of the in-phase component

N_Q ASE noise power spectrum density of the quadrature component

N_{MC} Number of MC sample functions

N_s Number of symbols

n_{sp} Spontaneous emission noise factor

P_0 Average power of the selected signal

P_{in} Accumulated Power of the selected signal

P_n ASE noise power

P_{LO} Local oscillator power

R_s Symbol rate

R_λ Photodetector responsivity

T Overall duration of the simulated signal

T_a Sampling time

T_s Symbol time

X_c Crosstalk level

$X_{c,max}$ Crosstalk level for 1 dB OSNR penalty

Chapter 1

Introduction

In the last years, with the exponential internet traffic growth due to the number of laptops, gadgets, applications and cloud services that demand more bit rate, fiber optic networks need to keep evolving to be able to support all the traffic that is being generated. Transmission techniques such as dense wavelength-division multiplexing (DWDM), allow fiber optic networks to answer this continuous demand of transporting more and more traffic, but an evolution on optical network nodes is just as important. In the past, going from manual switchboards to automated switches, presented a significant improvement in the routing and switching of signals in a network node, by making it faster, dynamic and more reliable. Reconfigurable optical add/drop multiplexers (ROADMs) technology, bring similar advantages to optical network nodes.

1.1   Evolution of Optical Network Nodes

Figure 1.1, shows the basic DWDM functions that optical network nodes need to have: multiplexing/demultiplexing optical signals with multiple wavelengths (a) and add/drop of individual wavelengths (b). Notice each line represents an individual wavelength.
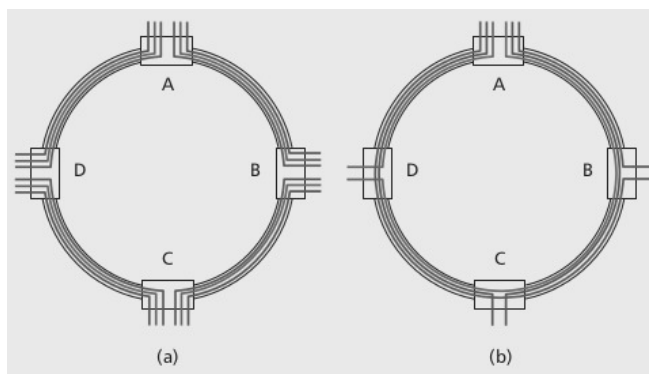

Figure 1.1: Basic DWDM functions: a) multiplexing/demultiplexing; b) add/drop [11].

Prior to ROADM technology, add/drop and routing operations of individual channels in a network node was a very challenging process. It required a demultiplexer to separate individual wavelengths at the node input, afterwards each individual wavelength had to be manually rearranged at an optical patch panel, before being recombined again into the desired output fiber, using an optical multiplexer, in order to be transmited to the next node [8]. Removing the need for manual fiber connections when changing add/drop patterns, greatly reduced the time required to implement these changes, contributing to an increase in network availability [11]. ROADMs are suited for DWDM metropolitan networks, with a large number of wavelengths and a significant bandwidth demand that is relatively unpredictable [13]. The versatility of ROADM-enabled DWDM systems, brought benefits for the network operator such as simpler network planning, installation and turn-up, as well as simplifying the process of adding new wavelengths to the network [11].

1.2 In-band Crossalk

In the physical layer of an optical network, crosstalk is one of the most important performance degradation factors. Many optical components that are present in optical networks, such as ROADMs, have imperfections [2]. These imperfections can translate into signal leaks, which can interfere with the selected signal and result in a system performance degradation. The worst case in terms of system performance degradation, happens when the leaked signal has the same nominal wavelength of the selected signal. This phenomenom is called in-band crosstalk, can be originated from different optical transmiters and cannot be eliminated through optical filtering.

In this dissertation, we will assess the degradation of the coherent receiver performance due to in-band crosstalk, using QPSK and 16-QAM signals.

1.3 Dissertation Organization

The dissertation is organized in the following order. The second chapter describes the coherent detection technique, the coherent detection receiver and some of its components, as well as its theoretical and simulated model. The method used to assess the bit error rate (BER) is presented, and some MC simulation aspects are discussed.

The third chapter focuses on the study of ROADMs, as well as some of its components, with special focus on the WSS. Several ROADM node features such as colorless, directionless and contentionless ROADM based nodes are described. Also, two different ROADM node architectures are studied: Broadcast-and-Select and Route-and-Select.

In the fourth chapter, two types of crosstalk are described, in-band crosstalk and out-of-band crosstalk. It is also explained how the crosstalk model was implemented in the MC simulation, in order to measure the impact of in-band crosstalk in the system performance, regarding the OSNR penalty. Weighted crosstalk metric concept and its mathematical description are also introduced in this chapter. The different WSS models used in the MC simulation are presented, and its filter shapes analyzed. Afterwards, the coherent receiver performance for both QPSK and 16-

QAM modulation formats, in the presence of in-band crosstalk which is introduced in a two-degree ROADM node, is assessed. In this assessment, two distinct metrics are used: unweighted crosstalk and weighted crosstalk. Additionally, a comparison between the results obtained by both metrics is presented.

The fifth and final chapter, summarizes the main conclusions drawn from this work, and suggests some topics for possible future work.

1.4 Main Contributions

In this work, some contributions relative to other studies in the field were introduced. The contributions with most relevance to the analysis performed in this work, are the following:

- Assessment of the impact of the in-band crosstalk on the coherent receiver performance, considering interferers with the same modulation format and same bit rate of the selected signal, routed through a ROADM node using unweighted crosstalk metric.

- Assessment of the impact of the in-band crosstalk on the coherent receiver performance, considering interferers with the same modulation format and same bit rate of the selected signal, routed through a ROADM node using weighted crosstalk metric.

- Comparison between the assessment of the OSNR penalty at the M-QAM coherent receiver due to insertion of in-band crosstalk in a ROADM node, using unweighted and weighted crosstalk metrics.

- Analysis of the advantages of using weighted crosstalk metric, when evaluating the M-QAM coherent receiver performance in terms of OSNR penalty, due to in-band crosstalk.

Chapter 2

Coherent Receiver Theoretical and Simulation Models

2.1 Introduction

In this chapter, in section 2.2, we will describe the coherent receiver components and present the receiver model used in the MC simulation. The coherent receiver model used in the MC simulation is described in section 2.3, and the theoretically derived statistics of the detected current at the optical coherent receiver output are also presented.

In section 2.4, the mathematical expression for the theoretical BER of M-ary QAM systems and the performance evaluation method used in this work are described.

The signals generation in the MC simulation is depicted in section 2.5, as well as a detailed description of the MC simulator.

The conclusions of this chapter are drawn in section 2.6.

2.2 Coherent Receiver Components

Coherent detection enables higher order modulations than direct-detection receivers such as M-ary Phase-Shift Keying (M-PSK) and M-QAM signals, resulting in a spectral efficiency increase. The information carried in the optical signal such as amplitude, frequency, phase and polarization, is converted to the electrical domain by coherent receivers with no information loss. The use of digital signal processing at the optical receiver compensates any linear impairment occurring during the transmission [1].

Another advantage of coherent detection is the use of Polarization Division Multiplexing (PDM) technique. This multiplexing technique increases spectral efficiency by transmitting two modulated signals in the same optical carrier, with the carriers being transmitted using orthogonal polarizations.

2.2.1 Optical Amplification

Optical amplification is necessary due to the signal attenuation which is introduced by several components in optical networks, such as multiplexers/demultiplexers, optical couplers/splitters, ROADMs, etc. This means that in optical networks, signal amplification is essential in order to compensate path losses. There is a consequence of amplification, namely, the addition of amplified spontaneous emission (ASE) noise to the signal [23]. The ASE noise power can be measured through the OSNR, which is defined by

$$OSNR = \frac{P_{in}}{P_{ASE}} \tag{2.1}$$

with P_{in} being the accumulated power of the selected signal, which includes the two states of polarization [6], P_{ASE} is the average ASE noise power and is defined for both noise polarizations by

$$P_{ASE} = 2N_{ASE}B_{OSA} \tag{2.2}$$

with B_{OSA} being the Optical Spectrum Analyzer (OSA) bandwidth, which usually is equal to 12.5 GHz [26]. The purpose of the OSA is to measure the OSNR at a particular wavelength, and B_{OSA} relates to the simulation bandwidth, B_{sim}, by [26]

$$B_{OSA} = \frac{B_{sim}P_{ASE}}{2P_n} \tag{2.3}$$

and P_n is the ASE noise power used in the simulation. The ASE noise Power Spectral Density function (PSD) of one polarization is expressed by

$$N_{ASE} = n_{sp}h\nu_0(g-1) \tag{2.4}$$

with n_{sp} being the spontaneous emission noise factor, h the Planck constant, ν_0 the optical carrier frequency and g the power gain. Notice that the ASE noise is considered to be an Additive White Gaussian Noise (AWGN).

2.2.2 Local Oscilator

The Local Oscilator (LO) is what allows the coherent receiver to decode the information in the I and Q components of the optical signal. Ideally, the LO frequency should be dimensioned to be as close as possible to the optical carrier frequency, increasing the coherent receiver performance [22]. For simulation purposes, the LO is considered to be synchronized with the optical frequency and the intensity noise is neglected. We define the LO signal as:

$$E_{LO}(t) = \sqrt{P_{LO}}e^{j\phi_{LO}(t)} \tag{2.5}$$

with $\phi_{LO}(t)$ being the phase of the LO and P_{LO} the LO optical power.

2.2.3   2 x 4 90°Hybrid

Figure 2.1 shows a 2 x 4 90°hybrid, which was choosen due to being the most commonly used hybrid configuration in optical communications. Notice the four 3 dB couplers and the 90°phase shift in the lower branch which allows the receiver to decode the I and Q signal components.
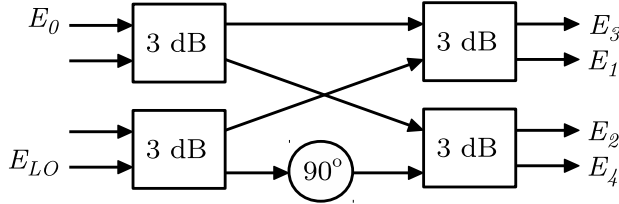
Figure 2.1: 2 x 4 90°hybrid configuration.

2.2.4   Polarization Beam Splitter

The purpose of the Polarization Beam Splitter (PBS) is to split the input Polarization-division Multiplexing (PDM) signal, P_{in}, into two components: vertical and horizontal. In ideal conditions, both components of the signal have equal power [26], $P_p = P_{in}/2$, with P_p being the average signal power of each PBS output. This will effect the P_{ASE} of each signal component, i.e., $P_{ASE,p} = P_{ASE}/2 = N_{ASE}B_{OSA}$, leading us to the mathematical expression for the OSNR of each polarization, $OSNR_p$, which is discribed by [6]

$$OSNR_p = \frac{P_p}{N_{ASE}B_{OSA}} = \frac{P_{in}}{2N_{ASE}B_{OSA}} \tag{2.6}$$

2.2.5   Photodetector

Each photodetector converts the received optical signal to an electrical signal. The photodetector responsivity, R_λ, can be described as [23]:

$$R_\lambda = \frac{I_p(t)}{P_{in}(t)} \tag{2.7}$$

with $I_p(t)$ being the current produced by the received optical power, $P_{in}(t)$, at the photodetector. We will consider that the photodetector responsivity is $R_\lambda = 1A/W$, resulting in $P_{in}(t) = |E_{in}(t)|^2$, where $E_{in}(t)$ is the electrical field incident on the photodetector.

2.2.6   Post-Detection Electrical Filter

After photodetection the coherent receiver has a low-pass filter, represented as $h(t)$ in Fig. 2.2, with the objective of improving the Signal-to-Noise Ratio (SNR) at the decision circuit input, by

7

reducing the noise and Intersymbol Interference (ISI) of the incoming signal. The filter shape is very important and needs to be carefully dimensioned to be as close as possible to the shape of the incoming signal (matched filter) [24].

2.3   Coherent Receiver Signal Analysis

The general setup of a coherent optical receiver is shown in Figure 2.2. The main differences between a direct optical receiver and a coherent optical receiver is the addition of a local oscilator, the use of four photodetectors instead of one, two subtractors and the hybrid. Notice that this model only takes into account one polarization.
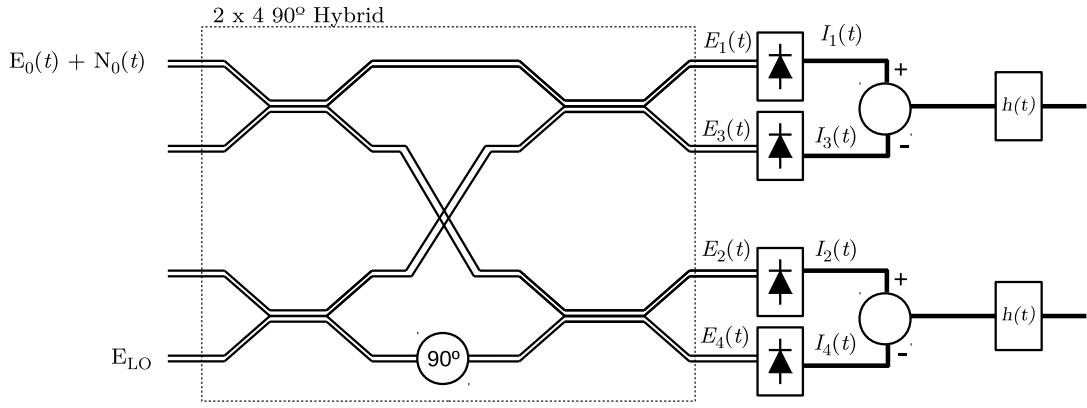
Figure 2.2: Coherent Optical Receiver model

In Fig. 2.2, $E_0(t)$ is the optical field of the selected signal, $N_0(t)$ is the *ASE* noise complex field, E_{LO} is the optical field of the local oscillator. E_1 to E_4 are the optical fields at the photodetectors inputs, which can be expressed as [6]:

$$E_1(t) = \sqrt{1-\epsilon}[E_0(t) + N_0(t)] + \sqrt{\epsilon}E_{LO} \tag{2.8}$$

$$E_2(t) = -\sqrt{\epsilon}[E_0(t) + N_0(t)] + \sqrt{1-\epsilon}E_{LO} \tag{2.9}$$

$$E_3(t) = \sqrt{(1-\epsilon)}[E_0(t) + N_0(t)] + j\sqrt{\epsilon}E_{LO} \tag{2.10}$$

$$E_4(t) = -\sqrt{\epsilon}[E_0(t) + N_0(t)] + j\sqrt{1-\epsilon}E_{LO} \tag{2.11}$$

The sign of the signal term originates from energy conservation whitin the lossless beam splitters with power transmission coefficient ϵ, ideally $\epsilon = 0.5$, and the multiplication by j is caused by the 90°phase shift of the LO [6]. After square-law photodetection, the output photocurrent in each photodetector is written, respectively, as:

$$I_1(t) = |E_1(t)|^2 = E_1(t)E_1^*(t) \tag{2.12}$$

$$I_2(t) = |E_2(t)|^2 = E_2(t)E_2^*(t) \tag{2.13}$$

$$I_3(t) = |E_3(t)|^2 = E_3(t)E_3^*(t) \tag{2.14}$$

$$I_4(t) = |E_4(t)|^2 = E_4(t)E_4^*(t) \tag{2.15}$$

where * stands for complex conjugate. By replacing $E_1(t)$ given by 2.8 in Eq. 2.12 we get:

$$\{\sqrt{1-\epsilon}[E_0(t) + N_0(t)] + \sqrt{\epsilon}E_{LO}\}\{\sqrt{1-\epsilon}[E_0(t) + N_0(t)]^* + \sqrt{\epsilon}E_{LO}^*\} \tag{2.16}$$

Multiplying the terms in 2.16 we get:

$$(\sqrt{1-\epsilon})^2[E_0(t) + N_0(t)][E_0(t) + N_0(t)]^* + \sqrt{\epsilon(1-\epsilon)}[E_0(t) + N_0(t)]E_{LO}^* + \sqrt{\epsilon(1-\epsilon)}[E_0(t) + N_0(t)]^*E_{LO} + [\sqrt{\epsilon}]^2E_{LO}E_{LO}^* = (1-\epsilon)[E_0(t)E_0(t)^* + N_0(t)N_0(t)^* + E_0(t)N_0(t)^* + N_0(t)E_0(t)^*] + (\epsilon)E_{LO}E_{LO}^* + \sqrt{\epsilon(1-\epsilon)}[E_0(t)E_{LO}^* + N_0(t)E_{LO}^* + E_0(t)^*E_{LO} + N_0(t)^*E_{LO}]$$

Knowing that $x = (a + ib)$ and $y = (c + id)$, with

$$xy^* + yx^* = 2ac + 2bd = 2Re\{xy^*\} \tag{2.17}$$

The expression for $I_1(t)$ is obtained:

$$I_1(t) = (1-\epsilon)[|E_0(t)|^2 + |N_0(t)|^2 + 2Re\{E_0(t)N_0(t)^*\}] + \epsilon|E_{LO}|^2 + 2\sqrt{\epsilon(1-\epsilon)}[Re\{E_0(t)E_{LO}^* + N_0(t)E_{LO}^*\}] \tag{2.18}$$

the calculation of $I_2(t)$, $I_3(t)$ and $I_4(t)$ follows a similar procedure of the one used for $I_1(t)$.

$$I_2(t) = \epsilon[|E_0(t)|^2 + |N_0(t)|^2 + 2Re\{E_0(t)N_0(t)^*\}] + (1-\epsilon)|E_{LO}|^2 - 2\sqrt{\epsilon(1-\epsilon)}[Re\{E_0(t)E_{LO}^* + N_0(t)E_{LO}^*\}]$$

$$(2.19)$$

$$I_3(t) = \epsilon[|E_0(t)|^2 + |N_0(t)|^2 + 2Re\{E_0(t)N_0(t)^*\}] + (1-\epsilon)|E_{LO}|^2 + 2\sqrt{\epsilon(1-\epsilon)}[Im\{E_0(t)E_{LO}^* + N_0(t)E_{LO}^*\}]$$

$$(2.20)$$

$$I_4(t) = \epsilon[|E_0(t)|^2 + |N_0(t)|^2 + 2Re\{E_0(t)N_0(t)^*\}] + (1-\epsilon)|E_{LO}|^2 - 2\sqrt{\epsilon(1-\epsilon)}[Im\{E_0(t)E_{LO}^* + N_0(t)E_{LO}^*\}]$$

$$(2.21)$$

With the two quadrature components and the two in-phase components, we now can obtain the received in-phase $I_I(t)$ and quadrature $I_Q(t)$ components which are in agreement with [6].

$$I_I(t) = I_1(t) - I_2(t) = 4\sqrt{\epsilon(1-\epsilon)}Re\{E_0(t)E_{LO}^* + N_0(t)E_{LO}^*\} \tag{2.22}$$

$$I_Q(t) = I_3(t) - I_4(t) = 4\sqrt{\epsilon(1-\epsilon)}Im\{E_0(t)E_{LO}^* + N_0(t)E_{LO}^*\} \tag{2.23}$$

Assuming an ideally balanced receiver ($\epsilon = 0.5$).

$$I_I(t) = 2Re\{E_0(t)E_{LO}^* + N_0(t)E_{LO}^*\} \tag{2.24}$$

$$I_Q(t) = 2Im\{E_0(t)E_{LO}^* + N_0(t)E_{LO}^*\} \tag{2.25}$$

Then, $I_I(t)$ and $I_Q(t)$ are filtered by an electrical filter that models the shape of the selected signal (matched filter) [6]. Notice that in Eqs. 2.24 and 2.25, the only important noise term is the beat term between the LO and the optical noise field, since both the beat terms between signal and optical noise and noise-noise beat term are eliminated using ideal balanced detection [6]. In the following, the variance of the LO-ASE beat noise is derived. By considering $h(t)$ as an electrical filter, the noise current $y(t)$ at the filter output for the $I_I(t)$ component is given by

$$y(t) = 2Re\{N_0(t)E_{LO}^*\} * h(t) \tag{2.26}$$

In order to calculate the variance of $y(t)$, we assume that a Gaussian optical noise field will remain Gaussian in the electric domain. This is true since the statistics of the noise optical fields are the same after the linear conversion performed by the optical coherent receiver of both optical signal and noise fields to electrical domain [6]. The variance of the beat noise term between the

LO and the ASE noise field is obtained by taking the expectation of the squared magnitude of the beat-noise term, $\sigma_{S_I, LO-N_{ASE}}^2 = E[|y(t)|^2]$. By assuming that $N_0(t)$ is a zero-mean stochastic process, we get [6]:

$$\sigma_{I_I, LO-N_{ASE}}^2 = 4E[|Re\{N_0(t)E_{LO}^*\} * h(t)|^2] \tag{2.27}$$

By knowing that $v * w(t) = \int_{-\infty}^{\infty} v(\lambda)w(t - \lambda)\, d\lambda$, we can write the convolution in its integral form:

$$\sigma_{I_I, LO-N_{ASE}}^2 = 4E[|\int_{-\infty}^{\infty} Re\{N(\tau)E_{LO}^*(\tau)h(t - \tau)\}\, d\tau|^2] \tag{2.28}$$

We can expand the real part in the integral of Eq. 2.28 into the sum of two complex conjugated terms using, $Re\{Z\} = (Z + Z^*)/2$,

$$\sigma_{I_I, LO-N_{ASE}}^2 = 4E[|\int_{-\infty}^{\infty} [N(\tau)E_{LO}^*(\tau)h(t - \tau) + (N(\tau)E_{LO}^*(\tau)h(t - \tau))^*]/2\, d\tau|^2] \tag{2.29}$$

Assuming $E[N(\tau)N(\tau')] = 0$ and by defining $E_{LO}E_{LO}^* = P_{LO}$

$$\sigma_{I_I, LO-N_{ASE}}^2 = 4P_{LO}\int_{-\infty}^{\infty}\int_{-\infty}^{\infty} E[N(\tau)N(\tau')]h(t - \tau)h(t - \tau')\, d\tau'\, d\tau \tag{2.30}$$

If we consider the noise to be white with power spectral density N_0 over the opto-electronic detection bandwidth, we can assume that $E[N(\tau)N(\tau')^*] = N_0\delta(\tau - \tau')$. Furthermore, by replacing $t - \tau$ for τ_1 and τ for $t - \tau_1$ we get:

$$\sigma_{I_I, LO-N_{ASE}}^2 = 4P_{LO}N_0\int_{-\infty}^{\infty}\int_{-\infty}^{\infty} \delta(t - \tau_1 - \tau')h(\tau_1)h(t - \tau')\, d\tau'\, d\tau_1 \tag{2.31}$$

According to the following convolution property $v(t) * \delta(t - td) = v(t - td)$ and converting to its integral form $\int v(\tau)\delta(t - td - \tau)\, d\tau = v(t - td)$, we get:

$$\sigma_{I_I, LO-N_{ASE}}^2 = 4P_{LO}N_0\int_{-\infty}^{\infty} h(t - \tau')h(t - \tau')\, d\tau' \tag{2.32}$$

By knowing that $\int h(t)^2 \, \mathrm{d}t = \int |H(f)|^2 \, \mathrm{d}f = 2B_e$ where B_e is the power equivalent bandwidth of the real-valued impulse response $h(t)$, we get the final expression for the variance of the beat noise term between the LO and the optical noise field [6]:

$$\sigma_{I_I,LO-N_{ASE}}^2 = 4P_{LO}N_0B_e \tag{2.33}$$

The variance of the LO-ASE beating noise in the Q component, $\sigma_{I_Q,LO-Nbeat}^2$, can be calculated using the same procedure.

2.4 Performance Evaluation Methods

In this section, we will derive the generalized expression for the BER of M-ary QAM systems, with M being a power of two. The BER will be metric used in this work to study the performance of the coherent receiver, and we will obtain that BER through a process called Direct Error Counting (DEC). We will also describe how the theoretical BER based on the Gaussian distribution was obtained.

2.4.1 Theoretical Bit Error Rate

In this work, we use two modulation formats, QPSK and 16QAM. Since both are M-ary QAM signals, we can describe the theoretical BER as [24]

$$BER_{QAM} = \frac{4}{\log_2 M}\left(1 - \frac{1}{\sqrt{M}}\right)Q\left(\sqrt{\frac{3}{(M-1)}SNR}\right) \tag{2.34}$$

with $Q(x)$ being the Q function defined in [25].

$$Q(x) = \frac{1}{\sqrt{2\pi}}\int_x^\infty \exp(-t^2/2)dt \tag{2.35}$$

We can describe the SNR as a function of the OSNR by [1]

$$SNR = \frac{2OSNRB_{OSA}}{R_s} \tag{2.36}$$

with R_s being the symbol rate. By replacing SNR in Eq. 2.34, we get

$$BER_{QAM} = \frac{4}{\log_2 M}\left(1 - \frac{1}{\sqrt{M}}\right)Q\left(\sqrt{\frac{6OSNRB_{OSA}}{(M-1)R_s}}\right) \tag{2.37}$$

2.4.2 Direct Error Counting

In this work, we will use DEC to measure the performance of the simulated optical communication system. The BER is essentially a ratio between the number of erroneous bits and the total number

of transmitted bits, and assuming a Gray mapping, it is defined by

$$BER = \frac{N_e}{N_{MC} N_s (log_2 M)} \tag{2.38}$$

with N_e being the number of errouneos bits, which are counted at the decision circuit, N_{MC} is the number of generated sample functions and N_s the number of symbols per sample function.

2.5   Implementation of the Monte Carlo Simulator

In this work, we develop a simulation tool implemented in Matlab to evaluate the performance of QPSK and 16-QAM optical signals in ROADM based optical networks, which is done by calculating the BER. In the following, some MC simulation aspects are explained with more detail. In this section, the generation os signals in the MC simulation is explained.

2.5.1   Signals Simulation

These signals are represented by discrete vectors (in time and in frequency), and the vector positions are indexed to time instants, in order to represent continuous signal samples. Both time and frequency vectors have the same number of positions, as shown schematically in Fig. 2.3 and 2.4, i. e., N_a number of samples per symbol times the number of symbols (N_s) that are being generated.

The symbols are generated in a random way and include all possible symbol transitions in one signal sample function.
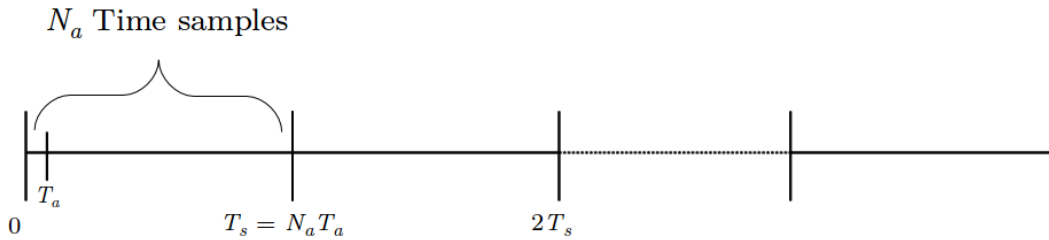
Figure 2.3: Simulated time vector.

In Figure 2.3, T_a is the sampling time defined by $T_a = T_s/N_a$, with T_s being the duration of a symbol.

Figure 2.4 shows the simulated frequency vector. In order to get the signal representation in frequency, we use the fast Fourier transform (FFT), which is an algorithm that calculates the discrete Fourier transform of the sampled discrete time signal. Positive frequencies are represented first and in the interval $[0, f_a/2 - \Delta f]$ and the negative frequencies in the interval $[-f_a/2, \Delta f]$. The sampling frequency is given by $f_a = 1/T_a$, and the frequency resolution Δf is defined by

Figure 2.4: Simulated frequency vector.

$$\Delta f = 1/N_a T_a \tag{2.39}$$

Using the fftshift Matlab function, the vector which represents the signal is shifted in frequency, so we can visualize the signal spectrum in its correct order.

2.5.2 Monte Carlo Simulation

In this subsection, we explain the MC simulation method used to estimate the BER of the M-QAM optical coherent receiver.
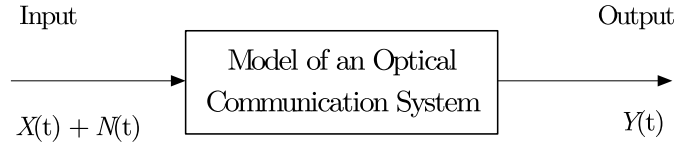
Figure 2.5: Block diagram of the Monte Carlo Simulation.

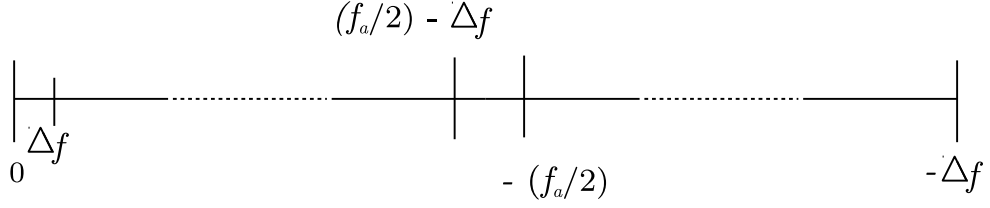In Figure 2.5, a simplified scheme of the MC simulation is presented. $X(t)$ is a random sequence of symbols, which is generated one time for all the iterations of the MC simulation. The randomness is introduced into the system by the noise component $N(t)$, which is added to $X(t)$, and the sum of both signals will be the input of our communication system modelled as a block. The signal at the output of the communication system, $Y(t)$, is the signal to be studied in order to obtain an accurate description of the statistical properties of $Y(t)$ and estimate the system BER. $N(t)$ represents ASE noise introduced by the EDFAs, and its noise field, in one polarization, is modeled as an additive white Gaussian noise (AWGN) process with in-phase, $N_I(t)$, and quadrature, $N_Q(t)$, components related by [17]

$$N(t) = 1/\sqrt{(2)}[N_I(t) + jN_Q(t)]. \tag{2.40}$$

Each noise component sample function is generated considering a zero mean and a variance equal to $N_0 f_a$, f_a being the equivalent ot the simulation bandwidth, B_{sim} [17].

Fig. 2.6 shows the flowchart that represents the simulator implemented in the computer to get the BER of the optical communication system.
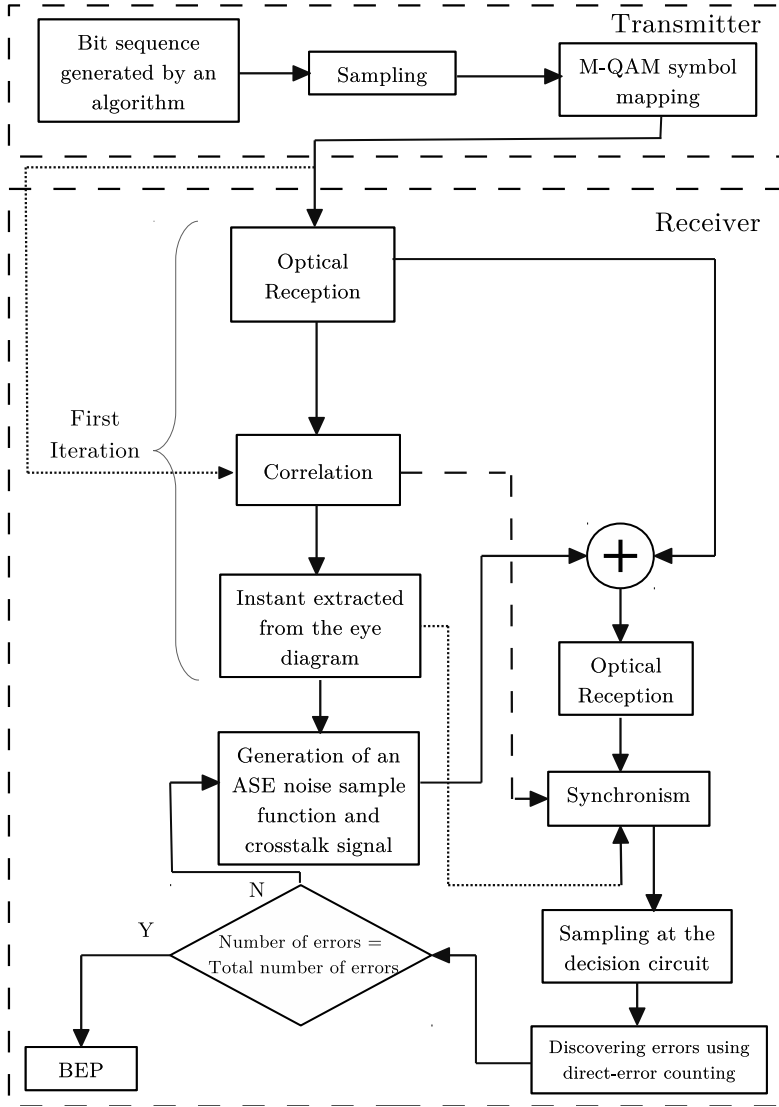
Figure 2.6: Flowchart of the MC simulation for a back-to-back configuration.

As we can see in Figure 2.6, the first step of the Monte Carlo simulation is to generate a pseudorandom sequence of symbols through an algorithm. This signal is then received by the coherent detector, and is correlated with the signal at the optical amplifier input. This will allow us to calculate the propagation delay along the optical reception, and construct the eye diagram at the decision circuit input, as is shown in Figure 2.7.(a). This delay is also important to synchronize

the received sequence with the original sequence.

(a)   (b)
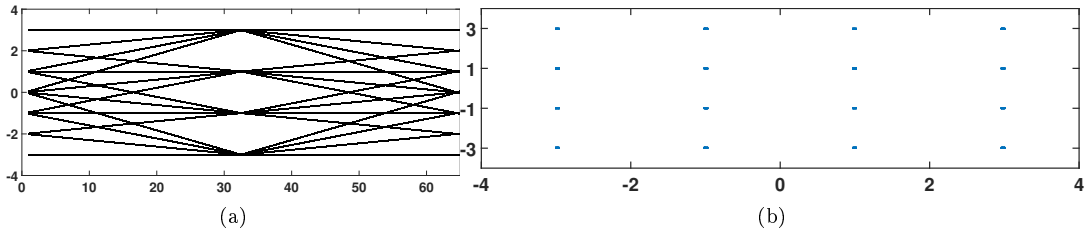
Figure 2.7: Eye diagram of the 16-QAM signal at the decision circuit input (a) and 16-QAM signal constelation at the decision circuit input (b) without noise.

Afterwards, by using the eye diagram we can obtain the optimum time sampling. Note that is taken into consideration the maximum eye opening, and it is the same sampling instant that will be used in all MC iterations to sample the received signals. The constelation of the detected signal is shown in Figure 2.7 (b), and this completes the first iteration of the MC simulation.

In the next iterations, a new random ASE noise sample function is generated everytime, and then added to the signal. The new signal with the noise component passes through the coherent receiver and is synchronized using the estimated propagation delay and sampled using the optimum sampling time, both obtained in the first iteration. We have at this point, a signal which possibly has errors, and will be compared to the ideal 16-QAM constelation through an algorithm. If there is an error, the variable N_e will be incremented untill it reaches the desired value. Therefore, this cyclical process ends when the number of erroneous bits are enough to a match predetermined target that matches a specified accuracy of the MC simulation.

(a)   (b)
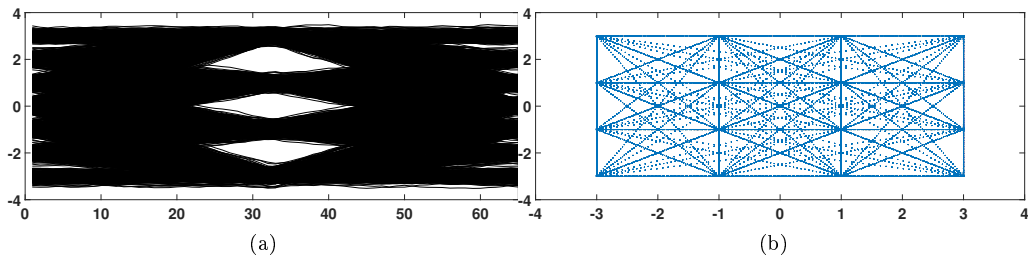
Figure 2.8: Eye diagram of 16-QAM signal with noise addition (a) and 16-QAM constelation of the detected signal with noise addition (b), both for a 20 dB OSNR.

Comparing Figure 2.7 (a) with Figure 2.8 (a) it is easy to identify the noise impact in the received signal. It is no longer possible to spot defined lines in the eye diagram due to ASE noise and in Figure 2.8 (b), instead of a single dot in the symbol positions just like we had in Figure 2.7 (b), we now have an aggregate of several dots in the symbol positions.

Finally, the simulation process will stop with the calculation of the BEP which is estimated through direct-error counting by

$$BEP = N_e/N_{it}(N_b - 1), \tag{2.41}$$

16

with N_{it} being the number of iterations of the MC simulator.

Using Eq. 2.41, we can estimate the DEC BER as a function of the OSNR for both QPSK and 16QAM modulation formats, exhbited in Fig. 2.9. It is visible that in both cases, the simulated curve overlaps the theoretical curve, validating the simulated results. In these simulations we used a bitrate of 42.8 Gbps and $B_0/R_s = 100$ for both modulation formats, 8192 symbols per MC iteration and $Na = 32$ for QSPK, 4096 symbols per MC iteration and $Na = 64$ for 16QAM.

(a)

(b)
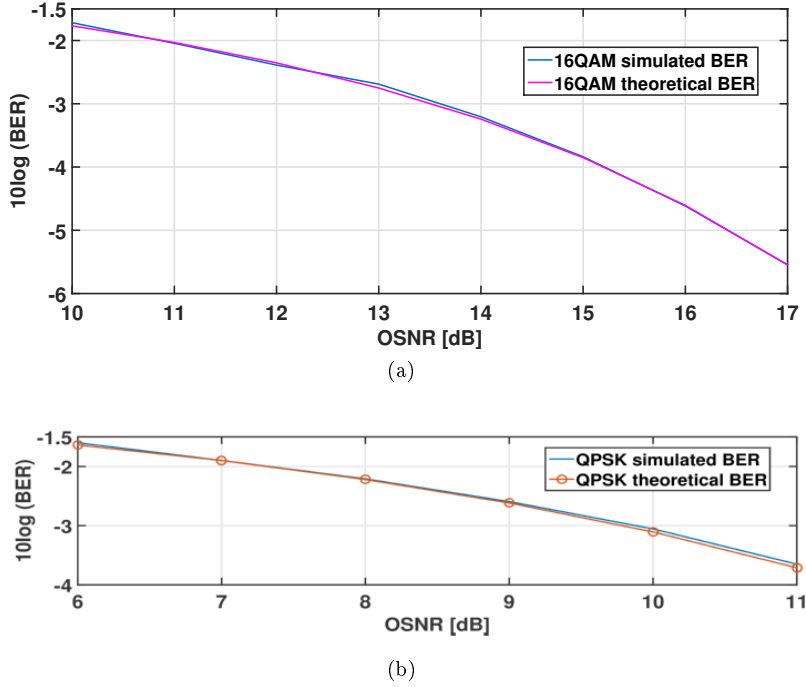
Figure 2.9: BER as a function of OSNR, using and ideal OF and EF, for the QPSK (a) and 16QAM (b) modulation formats.

2.6 Conclusions

In this chapter, we depict the optical coherent receiver and several of its components, as well as its model. When compared with direct detection receivers, coherent receivers enabled the use of higher order modulations, such as 16QAM and 64QAM, because it allows the detection of optical signals with information encoded in amplitude, phase and polarization components. These advantages come at the cost of an increase in complexity in the receiver end and the requirement of both transmitter and receiver to be synchronized. The mathematical analysis of the signals at the receiver input was exhibited and the statistical description of the ASE noise at the coherent receivers output was derived.

Afterwards, the evaluation method used in the MC simulation tool to access coherent receiver performance is explained. We also exhibit key aspect of the MC simulator, such as the data sequences generation, as well as the respective temporal and frequency representations.

Chapter 3

Reconfigurable Optical Add/Drop Multiplexer

3.1 Introduction

In this chapter, our goal is to explain the functionalities of several ROADM components, which will allow us to understand how do ROADM architectures work, and how did they evolve in order to address optical networks needs.

In section 3.2, crucial components of the ROADM such as the WSS, which are present in every ROADM architecture, are studied. Two degree ROADM architectures are described in section 3.3, as well as multidegree ROADM architectures in section 3.4.

The evolution of WSS towards several defining ROADM features such as coloress, directionless and contentionless ROADM nodes, are described in section 3.5.

Two different ROADM node architectures are described and compared in section 3.6.

The conclusions of this chapter are drawn in section 3.7.

3.2 ROADM Components

In this section, we will explain how some of the individual components that make part of a ROADM work, and why are they important to ROADM architectures.

3.2.1 Wavelength Selective Switch

WSS has been under constant development to support ROADM applications in multi-wavelength optical networks. Being a scalable technology, cost-effective, but also one of the most flexible solutions from an optical networking perspective, this makes the WSS the most widely used optical switch for ROADM applications [13].
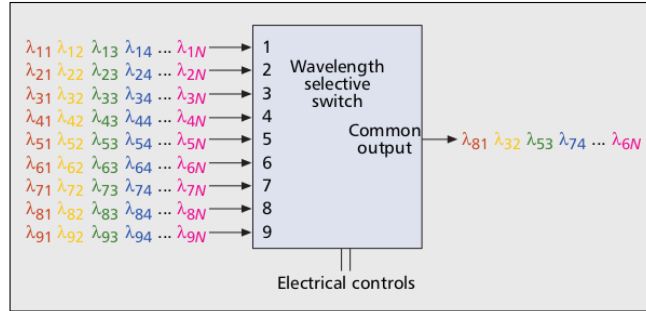
Figure 3.1: A 9 x 1 wavelength selective switch [8].

Before the WSS component appeared, the selection of individual wavelengths was not possible in the optical domain. This means that in an optical node, the input optical signal had to be converted to the electric domain in order to perform the selection of individual wavelengths. Then, the electrical signal had to be converted back to the optical domain, and finally routed to the next optical network node. WSS operates only in the optical domain, meaning that there is no longer the need for the optical-electrical and electric-optical convertions, saving time and complexity by requiring less hardware. What differentiates WSSs from the previous optical switches, is the ability to independently switch any wavelength to any port, without any restrictions imposed by the switching of other wavelengths [13].

This component can have multiple input fibers with different wavelenghts each, like it is shown in Figure 3.1, where we have 9 input fibers and select only the desired wavelengths to a common output fiber. WSS is a dynamic component since it can be programemd to add/drop different wavelengths. WSS configurations can be different from the one in Figure 3.1, existing N x 1, 1 x N, N x N or M x N configurations.

In addition to the flexibility advantages, WSSs also can atenuate the optical power of individual wavelengths at its output, making possible to equalize the optical power of the output wavelengths using variable optical attenuators (VOA) [8].

3.2.2 Different WSS technologies

There are four general classifications defined by two characteristics of the optical switch, as shown in Table 3.1. The first characteristic is the switching actuation technology, which in commercial devices is either Microelectromechanical systems (MEMS) or Liquid crystal (LC). The second characteristic is the number of pixels (switching elements) used to re-direct a single channel (i.e., a single pixel per channel or multipixels per channel) [8].

	MEMS	Liquid Crystal
Single Pixel/channel	Analog MEMS	Analog LC
Multi-pixel/channel	Digital Micromirror Device	LCoS

Table 3.1: WSS technologies

In Liquid Crystal array, optical signals are switched by manipulating the light polarization of the signals. This process advantages are the fact that it is economical and not complex. Scalability represents a problem for this implementation since optical performance degrades for higher port counts [8]. Similarly to liquid crystal array, LCOS uses light phase manipulation of the optical signals, and is flexible for different wavelength plans. The downside is being a complex implementation for calibration and maintaining performance stability [8].

MEMS technology steers the optical signals from the input port to the output port using micro mirrors of the MEMS chip. Scalability is a major advantage of this implementation, at the cost of not being an economical solution for low port counts [8]. Digital Micromirror Device (DMD), a polarization independent switch element, is a two state mirror array with more than 500 000 mirros/monolithic switch. Due to the small pixel size of (aprox. 10 μm), when integrated into a WSS this device uses many pixels per wavelength [8].

3.2.3   Optical Splitter/Coupler
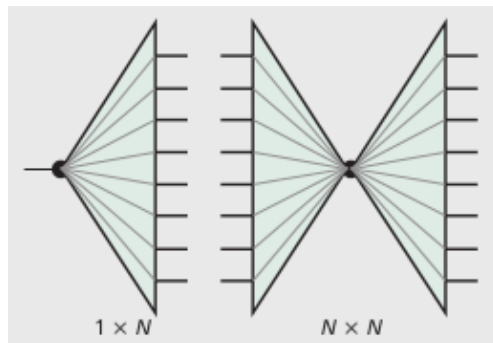
Figure 3.2: Optical splitter or coupler [12].

A 1 x N optical splitter receives an optical signal from a single input fiber, and distributes the optical power of the signal to the output fibers, with a power spliting ratio that is device-dependent, and typically designed to be wavelength-independent over the operating frequency of the ROADM. A typical optical splitter (1 x 2 fiber coupler), has ratios of 50/50 or 90/10 [12]. To make an optical coupler we just have to use the optical splitter in the opposite direction. In order to get N x N couplers, two 1 x N are combined. In Figure 3.2, 1 x N and N x N splitters/couplers are depicted.

3.2.4 Wavelength Splitter/Coupler

Figure 3.3: Wavelength splitter or coupler [8].

Another component that can be found inside a ROADM is the wavelength splitter, shown in Fig. 3.3. A wavelength splitter receives a single input fiber with different wavelengths and separates each wavelength to one 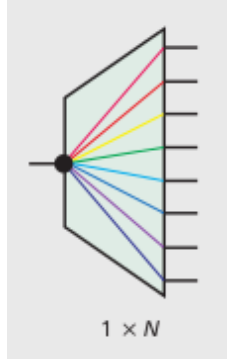of the many output fibers. An optical wavelength spliter operation in the reverse direction becomes an optical wavelength coupler.

3.3 Two-Degree ROADM Architectures

The first ROADM architectures were two-degree nodes, i.e., nodes with one entry point and one exit point. At its input, the ROADM shown in Figure 3.4 (a), has a multichannel DWDM fiber that is split to a 1 x 1 WSS and to a demultiplexer. The wavelengths that are meant to be dropped are routed to the multiplexer, while the ones that are meant to pass through the node are routed to the 1 x 1 WSS. The WSS has the task of selecting which wavelength(s) will pass, which wavelength(s) will be equalized and which ones will be blocked [8]. Note that the WSS also prevents the existence of duplicate wavelengths carrying the same traffic, by blocking wavelengths that are equal to the added wavelengths. Before the optical signal leaves the node, new wavelengths are added through passive combination after the multiplexer. Provided with the feedback given by the optical power monitor (OPM), the power of the added wavelengths is equalized using discrete variable optical attenuators (VOAs), and by the optical power equalization controls of the WSS. This means that the WSS is able to control the optical transfer function of each wavelength (optical channel).

Figure 3.4 (b) shows a similar ROADM implementation which uses a 2 x 1 WSS instead of the 1 x 1. The wavelengths are still passively combined at the multiplexer and the output of the multiplexer goes into the one of the WSS inputs. It is up to the WSS to select wavelengths from both input fibers, as well as routing these to the next network node. Note that in this architecture there is no longer the need for discrete VOAs, since the WSS equalizes the optical power of the added wavelengths [8].

The main advantage of these ROADM architectures lies on the fact that any wavelength passing through the node is routed and equalized in an automated fashion [8]. The next ROADM architectures will achieve the colorless property, where the ports of the add/drop structure do not
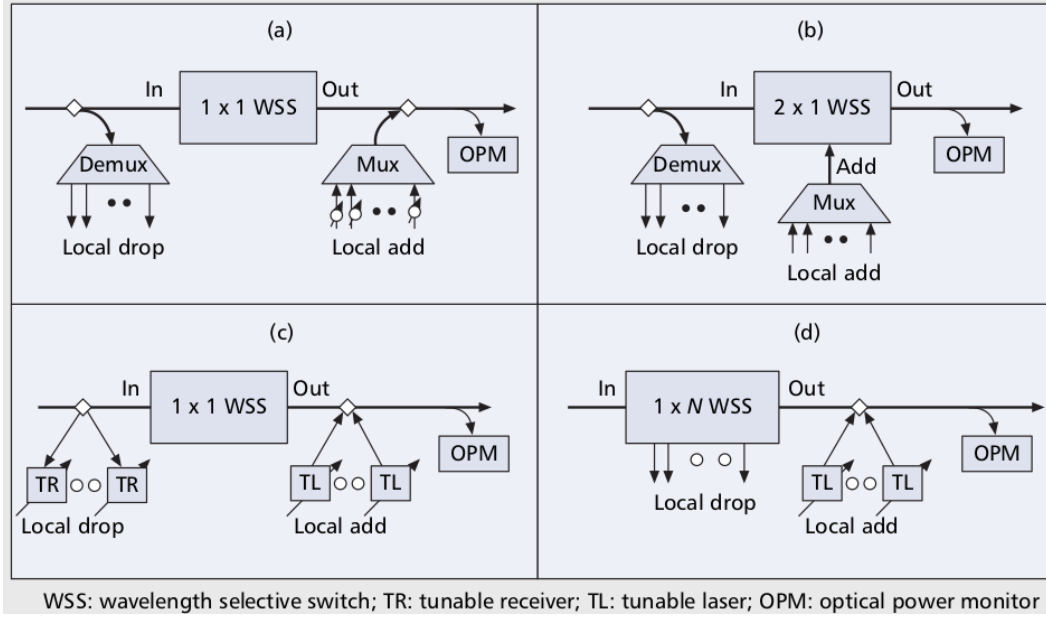
Figure 3.4: Two-Degree ROADM Architectures: a,b) fixed add/drop; c,d) colorless add/drop [8]

have a fixed wavelength assignment. The non-dynamic physical associations for the dropped and added wavelengths with the demux and mux ports are no longer a constraint due to the usage of tunable receivers (TRs) and tunable lasers (TLs). The tunable receiver is implemented by using the ouput of a tunable filter as a fixed receiver input. At the ROADM input, a single input fiber is passively splitted to the tunable receivers, which is represented in Figure 3.4 (c) as the local drop. Each one of these tunable receivers will select an individual wavelength. The local add is performed using tunable lasers, that passively add individual wavelengths to the output fiber of the node. In Figure 3.4 (d), we can see a variation of the previous architecture that uses a 1 x N WSS to dynamically select and drop individual wavelengths. A 1 x 9 WSS can drop any eight wavelengths, and use the ninth port for the DWDM output fiber [8]. Comparing fixed add/drop to colorless add/drop architectures, we can conclude that it is no longer needed to demultiplex all the incoming signals at each node, avoiding severe power losses to the express channels. Also, colorless architectures are most efficient in cases where it is possible to know beforehand the number of dropped/added wavelengths at a given node. This constraint comes from the resulting optical power losses of passive coupling or the fixed port size of the WSS [8].

3.4   Multi-Degree ROADM Architectures

Evolving from 2-degree ROADMs, a multidegree ROADM receives and routes optical signals from and to more than one node. Figure 3.5 (a) shows a segment of a multidegree ROADM with fixed add/drop structure. In this architecture, the first optical splitter routes the input DWDM fiber to other WSSs in the node, distributing the same input optical signal to every single one of the nodes intputs. The second splitter that is present in a multidegree node has the same purpose

of the splitter of the 2-degree node, to drop local traffic. The 1 x 1 WSS is replaced by a N x 1 WSS to receive traffic from the other DWDM input fibers of the node and local traffic as well. The size of the WSS is dictated by the order of the node, meaning that a four-degree node would require a 4 x 1 WSS.
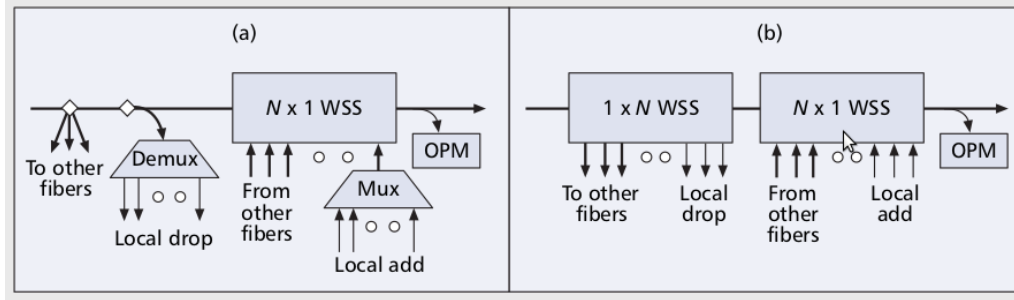

Figure 3.5: Multidegree ROADM architectures: a) fixed add/drop; b) colorless add/drop [8].

An example of a variation that implements colorless add/drop features is shown in Figure 3.5 (b). The tasks of the 1 x N WSS is to route the traffic from the DWDM input fiber to the remaining WSSs within the node, and to drop individual wavelengths [8]. The second WSS (N x 1) function, is to accept the traffic coming from other DWDM fibers, sent by the other WSSs in the node, and to add local wavelengths. This architecture brings advantages, such as more flexibility in wavelength assignment and routing, as well as reduced optical power budget, but comes at the cost of higher order WSSs. For instance, for an eight-degree ROADM, 16 WSSs (2 per segment) are required.

ROADM technology represents an important step of optical networks towards not only more flexibility in wavelength routing and wavelength assignment, but also to keep up with the increasing transmission capacity. This requires some properties from ROADMs such as being colorless, directionless and contentionless [12]. Figure 3.6 illustrates a 4-degree ROADM implementation with none of the proprieties described above (color and direction dependent ROADM).

By looking at Figure 3.6, we can see that the incoming channels received at the optical splitter, are distributed to the add/drop structure of the same degree and to the WSSs of all other degrees. A wavelength splitter separates the channels to the drop ports. To add channels, an optical coupler combines channels and sends the channels to a port on the WSS of the same degree [12]. Note that each wavelength is pre-assigned to a specific port. This is also commonly refered to as a colored design, given the add/drop structure is fixed [12].
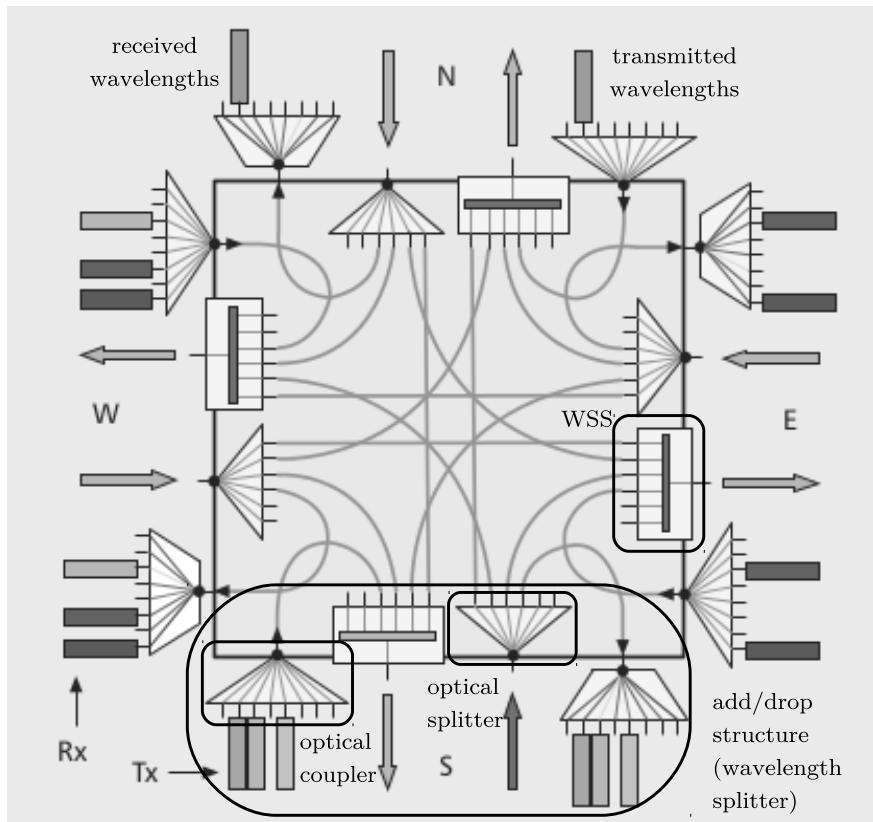
Figure 3.6: Color and direction dependent ROADM implementation [12].

3.5 ROADM features

3.5.1 Colorless ROADM Implementation

Contrarily to the colored design, in a colorless ROADM implementation there can be no fixed wavelenghts assignments to specific ports in the ROADM architecture. Colorless means that is possible to add/drop an optical signal independently of its wavelength, and this can be achieved by replacing the wavelength splitter by a WSS, as shown in Figure 3.7 [12].

The same optical coupler can be reused, since each transmitter sends out only one wavelength and the optical coupler is color independent. However, crosstalk between overlapping channels in the optical coupler can have a significant impact in the system performance. In order to overcome this, specifications to the laser side node (Tx) suppression ratio are necessary, or filtering the signal to reduce its bandwidth (and filter out noise) prior to the colorless combining [12]. In addition, a software protection for the system is required in order to prevent an incorrect wavelength assignment, which could interfere with an already existing channel of the same wavelength.

It should be noted that each degree still have specific wavelengths assigned. This means that
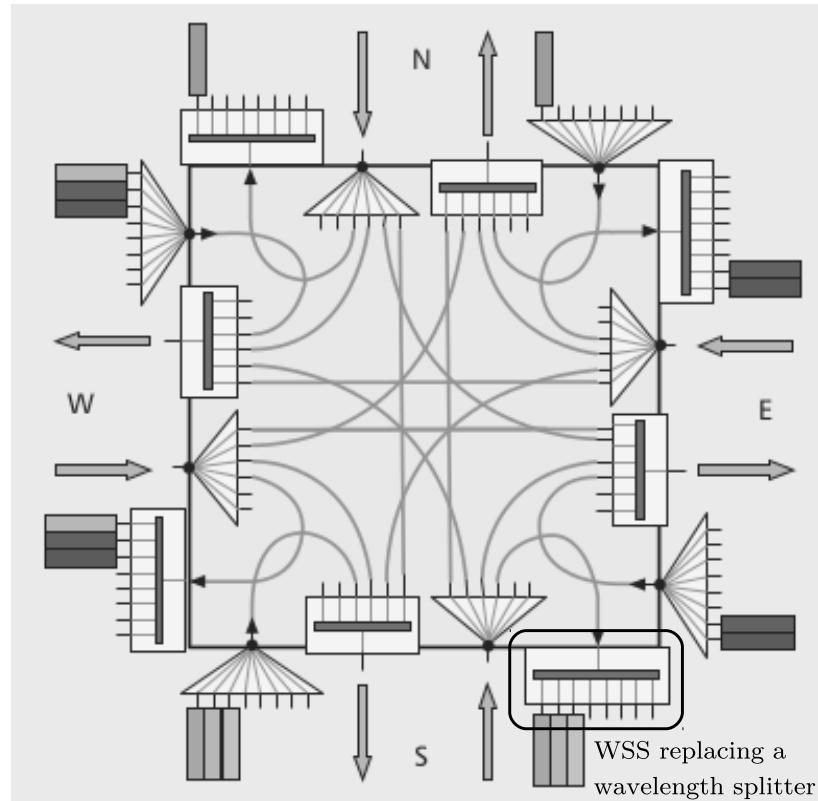
WSS replacing a
wavelength splitter

Figure 3.7: Colorless ROADM implementation [12].

if we want to use a specific wavelength in different degrees, this requires physical changes in the node.

3.5.2 Colorless and Directionless ROADM Implementation

A directionless ROADM implementation allows any channel to be added to any port, which can also be redirected to any node and vice-versa. This is possible by adding another 1 x M optical coupler to the add structure and another 1 x M WSS to the drop structure, as shown in Figure 3.8 [12].

Also, in Figure 3.8 we can see that only 2 of the 4 degrees have add/drop structures associated. This is type of solution reduces the number of add/drop structures and can be used in applications that do not require 100% add/drop [12]. The only limiting factor is that there cannot be repeated wavelengths in the same add/drop structure, meaning that wavelengths might have to be reasigned to other add/drop structures.
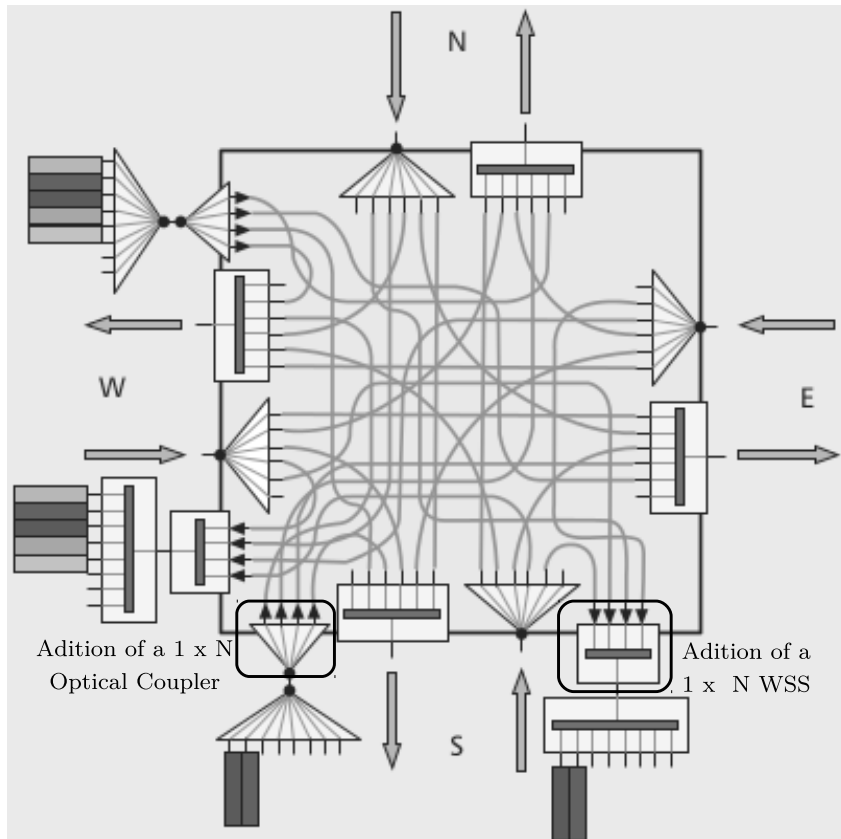
Figure 3.8: Colorless and Directionless ROADM implementation [12].

3.5.3 Colorless, Directionless and Contentionless ROADM Implementation

In the previously described ROADM implementation, we encountered a wavelength restriction in not being possible to have repeated wavelengths in the same add/drop structure. With a contentionless ROADM, we remove this restriction as long as the number of ports with repeated wavelengths is not greater then the number of degrees in the ROADM node.

As it is shown in Figure 3.9, this architecture allows us to have a single add/drop structure per node. In this particular case, this is implemented by having a M x N WSS that can switch any wavelength from an input port to any output port that is not using the same wavelength [12].

Note that the wavelength restrictions that colorless, directionless and contentionless ROADMs remove, are only true for the add/drop structure. If we look at network level these constraints still exist, since in a single mode fiber we cannot send repeated wavelengths. The major advantage brought by contentionless design is dinamic/automatic wavelength assignment, which reduces wavelength congestion.
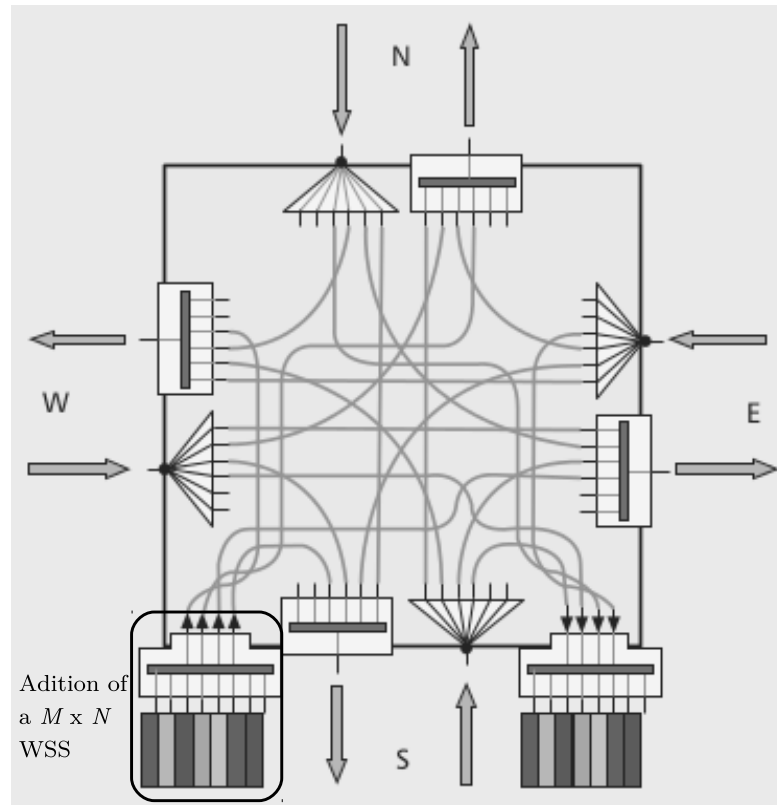
Figure 3.9: Colorless, Directionless and Contentionless ROADM implementation [12].

3.6 ROADM Node Architectures

There are different architectures when it comes to ROADM nodes. In this section we will explain the architectures Route-and-Select (R&S) and Broadcast-and-Select (B&S). We will also compare both architectures in terms of OSNR penalties versus the number of ROADM nodes that the optical signal passes through, and in which situations it is advantageous to use the B&S or the R&S architecture.

3.6.1 Route-and-Select (R&S)

By looking at Figure 3.10, R&S nodes use 2 WSSs per ROADM node, with the signal being selectively routed from the first WSS to the second WSS. Consequently, the desired signals are passively passed/blocked by the second WSS.

Figure 3.10: N-degree Route-and-Select node

3.6.2   Broadcast-and-Select (B&S)

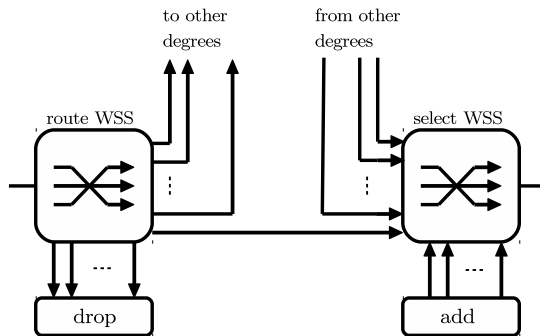Figure 3.11 shows a B&S node architecture, which uses one passive optical splitter and one WSS per ROADM node. All the signals at the splitter input are broadcasted to all the output ports of the splitter, which is connected to the input ports of the WSS. It is at the input ports of the WSS that the signals are passively passed or blocked [19].
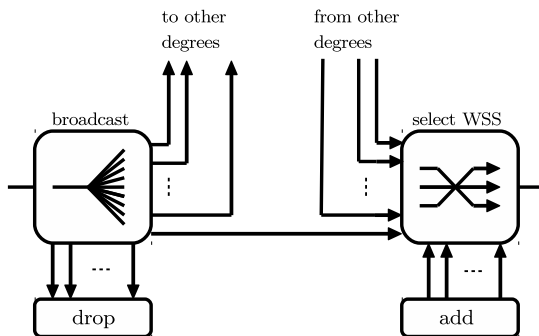
Figure 3.11: N-degree Broadcast-and-Select node

By only using 1 WSS, B&S architecture advantages come from reduced optical and electronic complexity, cost and power consumption. This solution disavantages come from the fact that it lacks scalability, due to reduced isolation on the blocking ports, as well as increased insertion loss for higher port counts (e.g., N=9) [19].

3.6.3   R&S versus B&S

According to [19], for ROADM nodes with 9 or fewer degrees of connectivity, the B&S architecture have lower overall system penalties than R&S. It is safe to conclude that in this particular ROADM node setup, B&S architectures should be used instead of R&S architectures. R&S archi-

tectures should be used for higher port counts, since due to B&S ROADMs having higher insertion loss, additional amplification is required, introducing more ASE noise [19].

Note that all the conclusions above are made in an environment with no crosstalk. If we introduce crosstalk, we conclude that R&S is much more robust to crosstalk since it brings no additional degradation due to higher isolation of R&S configuration. The same cannot be said about B&S nodes, even though crosstalk addition only represents a minor OSNR penalty increase when compared to the curve without crosstalk in [19]. It is expected that this crosstalk penalty will become more relevant for higher port nodes.

3.7 Conclusions

In this chapter, several ROADM components were studied, as well as several ROADM architectures. We explained how it was possible to go from two-degree ROADMs to multi-degree ROADMs, which is directly tied with the evolution of different WSS technologies. The vital role of the WSS in enabling several ROADM features such as colorless, directionless and contentionless ROADMs is also presented, which eliminate several wavelength routing constraints, present in other ROADM architectures. These ROADM features allow a more dynamic and efficient wavelength assignment in each node, reducing wavelength congestion in the network.

Two different ROADM node architectures were described and studied. The advantages and the disavantages of both architectures were discussed, as well as which network scenario, such as, the number of nodes in the network and how many ports per node, suited the most to each ROADM node architecture.

Chapter 4

In-band Crosstalk Impact in ROADM Based Networks

4.1 Introduction

In this chapter, the performance of a M-QAM coherent receiver impaired by in-band crosstalk in a network with ROADM based nodes is studied.

In section 4.2, the different crosstalk types are described and the implementation of the in-band crosstalk in the MC simulation is explained. The validation of the in-band crosstalk model is demonstrated in subsection 4.2.1.

In section 4.3, the concept of weighted crosstalk as well as its mathematical description are presented.

Different WSSs with specific filter shapes used in the MC simulation are described and analyzed in section 4.4. Each filter shape characteristics is also analyzed.

In section 4.5, we present the studies of the in-band crosstalk impact and its respective simulation results for one ROADM node with one interferer (WSS 2x1). Finally, the conclusions of this chapter are presented in section 4.6.

4.2 Crosstalk Simulation Model

ROADM components such as optical splitters/couplers, de/multiplexers and WSSs, originate signal leakages due to imperfect isolation [2]. Crosstalk signals are signal leakages that occur in optical network nodes, which can lead to system performance degradation. Figure 4.1 illustrates two types of crosstalk signals, out-of-band crosstalk and in-band crosstalk.

Out-of-band crosstalk occurs when the interferer and the selected signal have different nominal wavelengths, λ_0 and λ_{XT}. A well designed optical filter can remove the effect of the interferer, as it is shown in Fig. 4.1.a). If the interferer is centered at the same nominal wavelength of the selected signal, $\lambda_{XT} = \lambda_0$, as shown in Fig. 4.1.b), we are in presence of in-band crosstalk. This

type of crosstalk leads to a higher power penalty due to crosstalk, since the interferer cannot be eliminated through optical filtering [2].
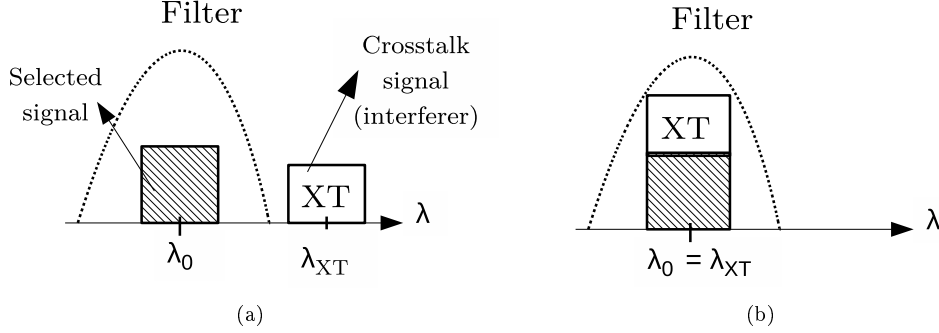

Figure 4.1: Crosstalk Types: out-of-band crosstalk (a) and in-band crosstalk (b).

The optical signal electrical field which arrives at the input of the coherent receiver can be analytically written by

$$E_{r_{filtered}}(t) = [E_0(t) + \sum_{i=1}^{N_x} E_{x,i}(t)e^{j\phi_{\varepsilon,i}} + N_0(t)] * h_0(t) \tag{4.1}$$

where $E_0(t)$ is the electrical field of the selected optical signal, $N_0(t)$ is the ASE noise, $E_{x,i}(t)$ is the electrical field of the i-th interfering signal, $\phi_{\varepsilon,i}$ is the phase error between the selected signal and interfering signal, and $h_0(t)$ is an optical filter. The crosstalk level $X_{c,i}$ of each interferer is defined as [18]

$$X_{c,i} = \frac{P_{x,i}}{P_0} \tag{4.2}$$

with $P_{x,i}$ and P_0 being the average powers of the i-th interferer and the selected signal, respectively.
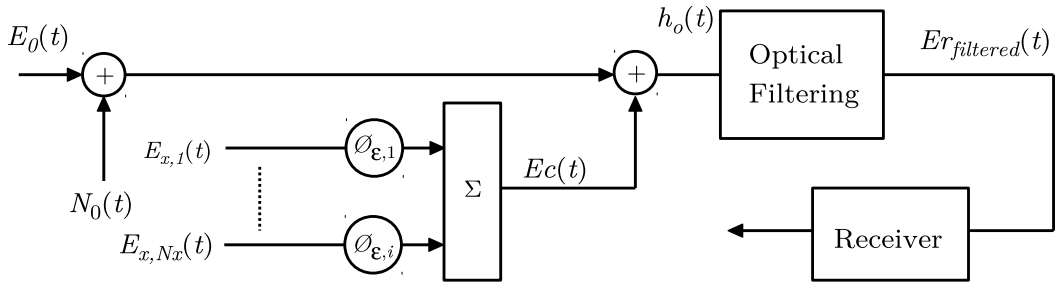

Figure 4.2: Crosstalk simulation model for one sample function of in-band crosstalk and ASE noise in one polarization direction.

Figure 4.2 exhibits the model used in the MC simulation to study the impact of in-band

crosstalk on the coherent receiver. In each MC simulation iteration, N_x interferers are generated, summed and then added to the selected signal, $E_0(t)$, together with the ASE noise, $N_0(t)$. Each interferer can be expressed mathematically by $E_{x,i}(t) = \sqrt{X_{c,i}}E_0(t)$. The QAM symbols that compose the selected signal and the interferers are generated randomly in each iteration of the MC simulation. Each crosstalk signal sample function average power is changed accordingly with Eq. 4.2. The phase difference $\phi_{\varepsilon,i}$ is modeled with an uniform distribution within the interval $[0, 2\pi[$. The interferers will then be summed and originate the crosstalk signal, $E_c(t)$. The signal which is now composed of the selected optical signal, ASE noise and in-band crosstalk will be filtered by the optical filter, $h_0(t)$, resulting in the optical signal at the receiver input represented in Fig. 4.2 by $E_{r_{filtered}}(t)$, whose electrical field is given in Eq. 4.1.

4.2.1 Validation of the MC Simulator

In the MC simulator, the degradation caused by interfering crosstalk signals is evaluated by measuring the OSNR penalty at a BER of 10^{-3} [4]. The first step is to obtain the crosstalk level associated with a 1 dB OSNR degradation, which we define as $X_{c,max}$. For every modulation coding scheme (MCS), $X_{c,max}$ is estimated by discovering the OSNR that leads to a BER of 10^{-3} in the absence of crosstalk. Then, the OSNR corresponding to $X_{c,max}$ is compaired with the OSNR that leads to a BER of 10^{-3}, but in the presence of crosstalk. The crosstalk level interval, $[-40, -5]$, is chosen with the objective of achieving BER estimates within the interval $[10^{-4}, 10^{-2}]$. The difference between the OSNR in the absense of crosstalk and the OSNR in the presence of crosstalk, will give us the OSNR penalty due to the interfering crosstalk signals.

Similar values of OSNR penalty are observed when comparing the results of Fig. 4.3 with the results exhibited in [4], i.e., for a 1 dB OSNR penalty we get a crosstalk level of about -16 dB for QPSK and -23 dB for 16-QAM, hence, validating the MC simulator. It should be noted that a back-to-back coherent receiver using QPSK and 16-QAM, both coded at 21.4 GBaud and considering a single interfering crosstalk signal is the configuration used both in [4] and in our MC simulation.
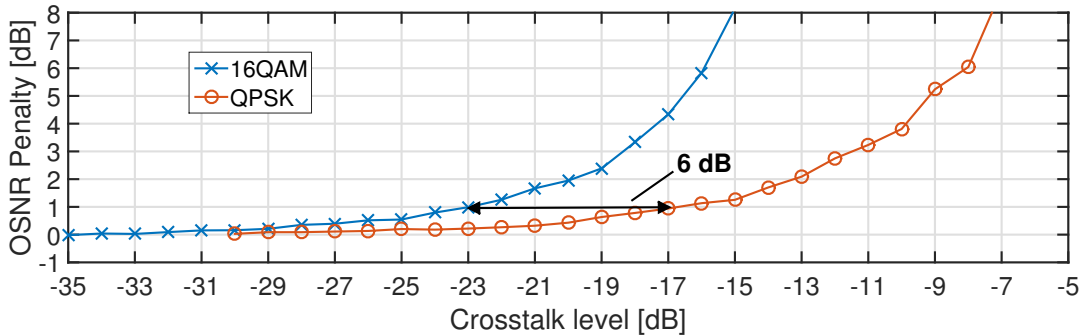

Figure 4.3: OSNR penalty as a function of the crosstalk level for a single interfering crosstalk signal with QPSK and 16-QAM modulation formats, coded at a symbol rate of 21.4 GBaud.

Regarding the performance impact of crosstalk signals in both MCSs, a better performance is

observed using QPSK, about 6 dB improvement in crosstalk level for a 1 dB OSNR penalty. In order to obtain an OSNR penalty of 1 dB, a higher crosstalk level is required using QPSK instead of 16-QAM, making QPSK the most robust modulation format to in-band crosstalk.

4.3   Weighted Crosstalk

When dealing with in-band crosstalk signals, the spectral shape of the interferer which may or not be different from the selected signal spectral shape, is usually not taken into account [20]. This leads to the definition of unweighted crosstalk power ratio given by

$$X_{c,i} = P_{x,i}/P_0 = \int_{-f_0}^{f_0} S_x(f)df \Big/ \int_{-f_0}^{f_0} S_0(f)df \qquad (4.3)$$

where $P_{x,i}$ is the total power of the i-th interfering signal, P_0 is the selected signal power and f_0 is the frequency range, $[-f_0, f_0]$, that covers the bandwidth of the signals at the detector input [3].

As shown in Fig. 4.4, when a signal at a specific wavelength, which we refer as the selected signal, is added at the ROADM node, another signal at the same wavelength, named as the interferer, should be blocked by a blocking filter with a power transfer function $|H(f)|^2$ [20]. $S_0(f)$ and $S_x(f)$ represent the power spectral densities of the selected signal and interferer, respectively.
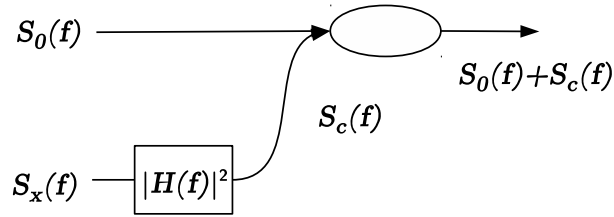
Figure 4.4: Schematic of the add operation in a ROADM node based on a 2x1 WSS.

So, the definition of the crosstalk power ratio should take into account the power spectral density (PSD) of the filtered crosstalk signal, denoted in Fig. 4.4 as $S_c(f) = |H(f)|^2.S_x(f)$, in order to deal with the spectral shape of the blocking filter. This led to the definition of the weighted crosstalk power ratio [20]

$$X_{wc} = \frac{P_{Xw}}{P_0} = \frac{\int_{-f_0}^{f_0} S_c(f).W(f)df}{\int_{-f_0}^{f_0} S_0(f)df} \qquad (4.4)$$

where the weight function $W(f)$ is defined as [3]

$$W(f) = k.S_0(f) \qquad (4.5)$$

and takes into account that spectral content around the channel center has significantly more

impact than near the channel edges. In Eq. (4.5) k is a scaling factor. This scaling factor k is obtained considering in Eq.(4.5) that the selected and the crosstalk signals have the same spectral shape. If $\alpha S_0(f) = S_c(f)$ [20], where α is an attenuation coefficient, by solving Eq.(4.5) in relation to k we have

$$k = \frac{\int_{-f_0}^{f_0} S_0(f)df}{\int_{-f_0}^{f_0} {S_0}^2(f)df} \tag{4.6}$$

By replacing k in Eq.(4.4), we get the final expression for the weighted crosstalk power ratio [3]

$$X_{wc} = \frac{P_{Xw}}{P_0} = \frac{\int_{-f_0}^{f_0} S_c(f).S_0(f)df}{\int_{-f_0}^{f_0} {S_0}^2(f)df} \tag{4.7}$$

4.4   WSS Model

In this section, the different blocking filters used in the simulation, to study the impact of in-band crosstalk in the MC simulation are described. By using blocking filters with different power transfer functions, we can simulate different WSS models and get a wider range of results. We consider that ROADM nodes have a fixed grid where each channel has a 50 GHz bandwidth [20].

4.4.1   Filters with −5 dB amplitude in the rejection bandwidth

(a) Filter 1   (b) Filter 2
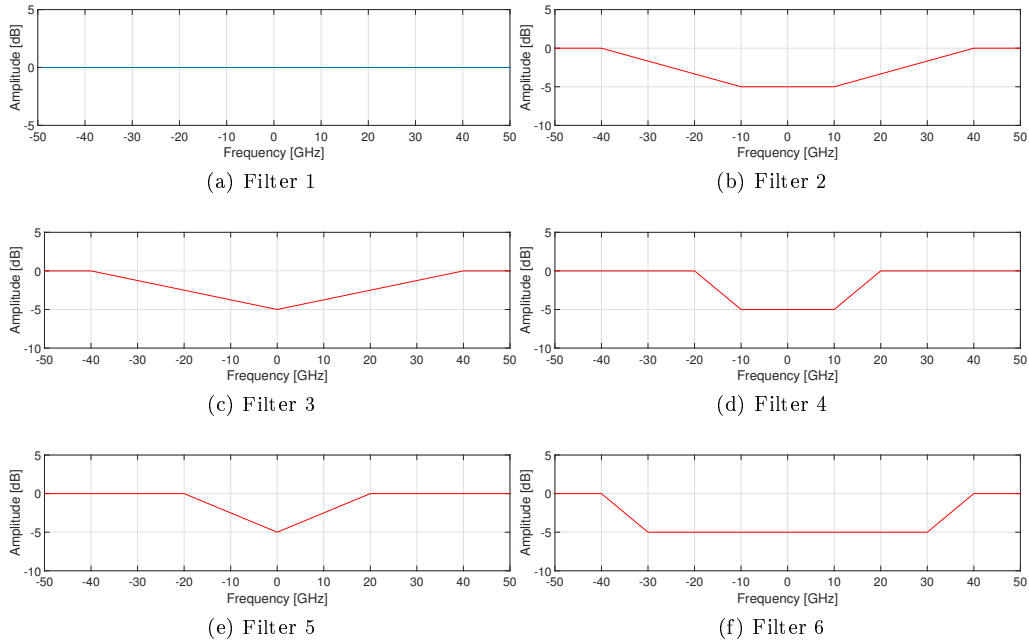
(c) Filter 3   (d) Filter 4

(e) Filter 5   (f) Filter 6

Figure 4.5: Filters with −5 dB amplitude in the rejection bandwidth.

Figure 4.5 shows the shapes of the blocking filters with attenuation of −5 dB in the rejection bandwidth. Note that filter 1 is equivalent to the absence of a blocking filter. This corresponds to a worst case scenario, where in-band crosstalk has a major impact on the receiver performance and is used as a reference case.

Analysing the filter shapes, it is safe to say that filter 6 will exhibit the best performance, due to its larger and centered rejection bandwidth (65 GHz at −3 dB). In contrast, we will see that filter 5 will be responsible for the worst performance, if we exclude filter 1. This is due to filter 5 having a very narrow rejection bandwidth (15 GHz at −3 dB), which will result in more crosstalk power leakage and, consequently, in an increase of the OSNR penalty due to crosstalk.

Filters 3 and 5 have very similar shapes and their main difference is in the width of the rejection band. Filter 3 has a rejection bandwidth of approximately 30 GHz at −3 dB, twice the bandwidth rejection width of filter 5. Both filters 2 and 4 are also similar in shape, differing in the rejection bandwidth range, with filter 2 rejection bandwidth being close to 40 GHz at −3 dB and filter 4 with around 30 GHz at −3 dB.

4.4.2 Filters with −10 dB amplitude in the rejection bandwidth

(a) Filter 1   (b) Filter 2

(c) Filter 3   (d) Filter 4
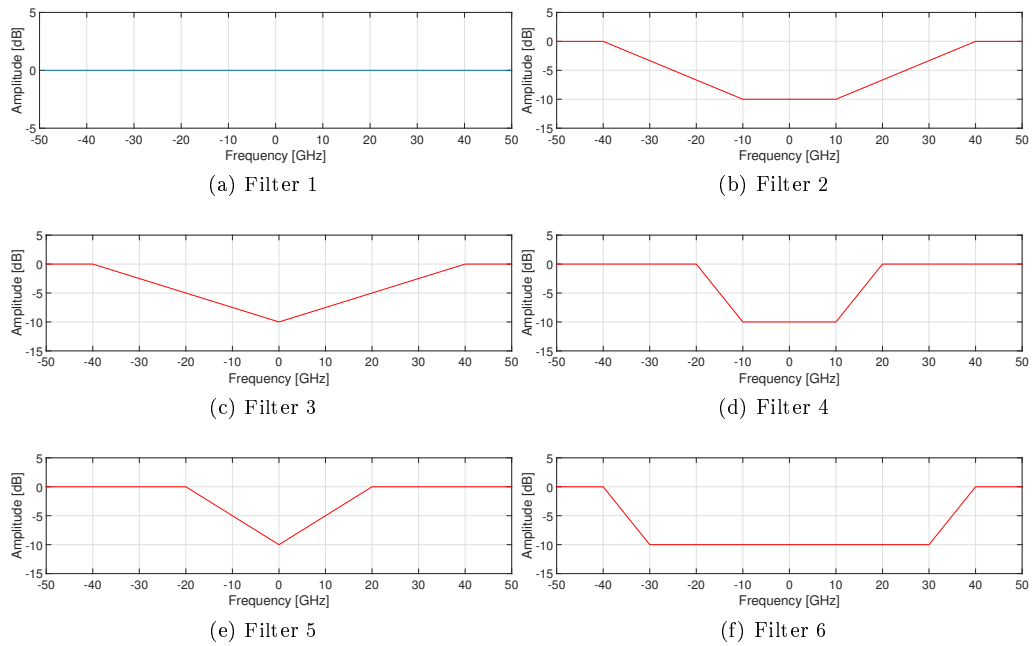
(e) Filter 5   (f) Filter 6

Figure 4.6: Filters with -10 dB amplitude in the rejection bandwidth. Filter 1 (a) to Filter 6 (f).

Figure 4.6 shows the filter shapes of the filters with attenuation of −10 dB in the rejection bandwidth. Notice that filter 1 corresponds to no blocking filter.

Notice that filter 2 and filter 4 are ideal models respectively of filters 2 and 4, used in Fig. 8 (b) in [20]. In the next section we will compare the results obtained with these filters with the results presented in [20], with real filters.

Regarding the filters shape, what has been stated for the filters with −5 dB of rejection bandwidth, remains true for the filters with −10 dB. As expected, filters with a rejection bandwidth amplitude of −10 dB will have better results regarding the OSNR penalty when compared to their respective pairs with −5 dB amplitude in the rejection bandwidth, due to the lower crosstalk introduced.

4.5 Impact of In-Band Crosstalk due to 1 WSS 2x1

In this section, we will study the impact of in-band crosstalk on the receiver performance using the OSNR penalty, considering one interferer in a ROADM node modeled by a WSS 2x1. Two MCSs are used, QPSK and 16QAM at 24.6 Gbps. We assume that both the selected signal and interferer have the same MCS. The OSNR penalty will be estimated considering the unweighted and weighted crosstalk, definitions given in eqs. 4.3 and 4.4, respectively.
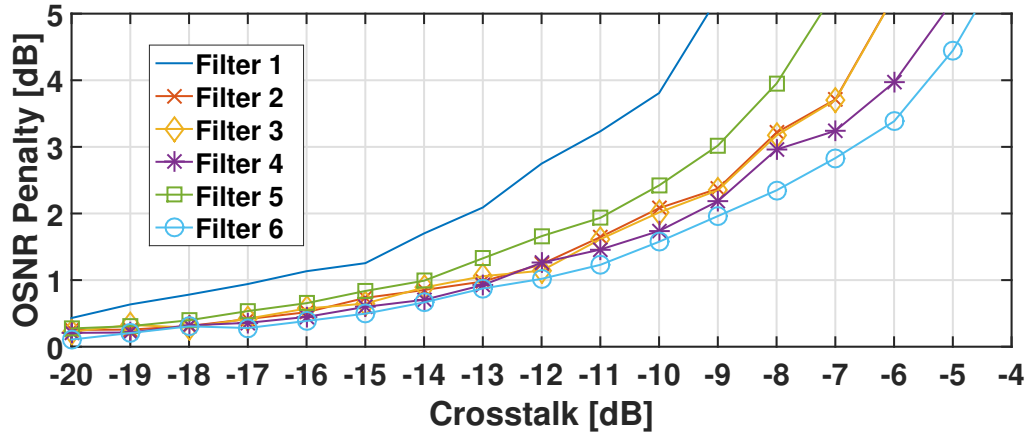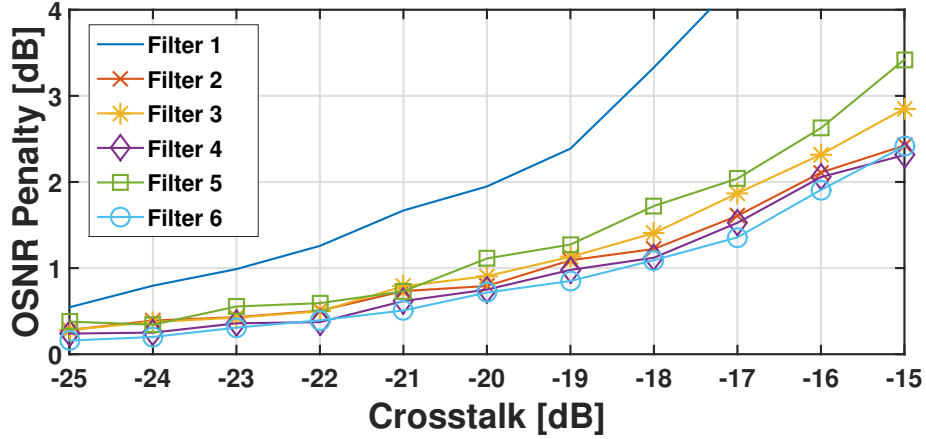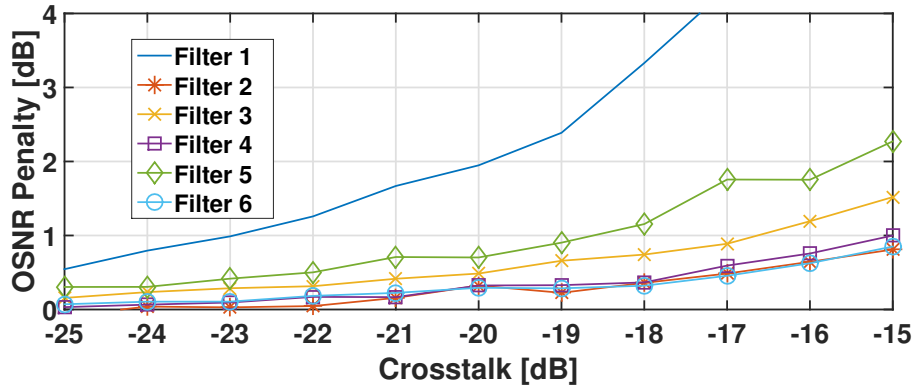

(a)
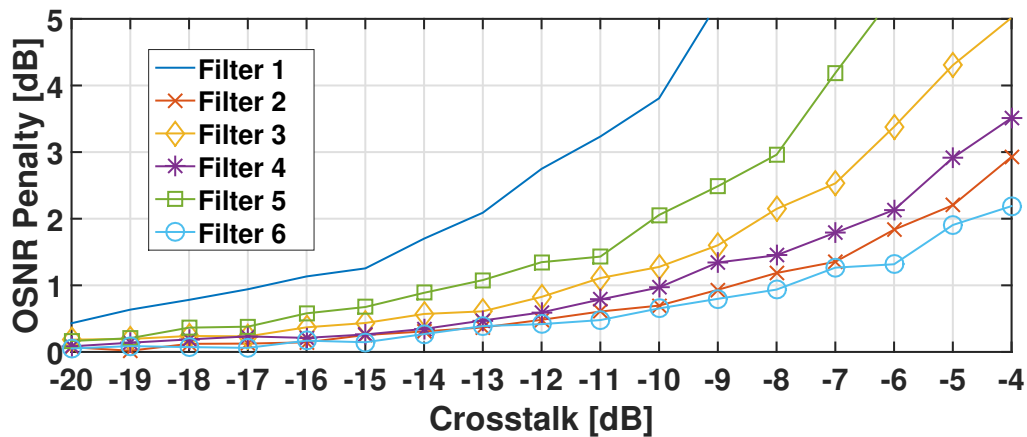
(b)

Figure 4.7: OSNR penalty as a function of the unweighted crosstalk with QPSK for $BER = 10^{-3}$ with −5 dB filter (a) and −10 dB filter (b).

Figure 4.7 shows the OSNR penalty as a function of the crosstalk level power ratio considering the unweighted crosstalk definition with QPSK modulation, using -5 dB and -10 dB blocking filters, respectively. Notice filter 1 curve in Fig. 4.7 (b) is in agreement with [20]. Figure 4.8 shows similar studies, but for the 16QAM modulation format.

(a)

(b)

Figure 4.8: OSNR penalty as a function of the unweighted crosstalk with 16QAM for $BER = 10^{-3}$ with -5 dB filter (a) and -10 dB filter (b).

As we stated before, ideal filters 2 and 4 are close to the real filters used in [20]. For filter 2 in [20], for a 1 dB OSNR penalty, a value of -8 dB of crosstalk level is achieved, while in our simulation it is observed a value of -8 dB for the same scenario. The difference of -0.8 dB can be explained by the fact that the obtained curves in the simulations are a snapshot of the last iteration, which occurred when the stoping criteria was met (100 errors). Given the crosstalk signal and the noise addittion are random processes, generated in each iteration, both introduce small variations between each iteration in the simulations. For filter 4, with a 1 dB OSNR penalty, we get a crosstalk level of -10 dB, in agreement with [20]. Note that this is only true for QPSK and -10 dB filters, since the scenarios for 16QAM and the -5 dB filters were not considered in [20].

Unweighted Crosstalk			
Modulation	WSS Filter	WSS Type	
		−5 [dB]	−10 [dB]
QPSK	Filter 1	−17	−17
	Filter 2	−13	−8.8
	Filter 3	−13.1	−11.5
	Filter 4	−12.9	−10
	Filter 5	−14	−13.5
	Filter 6	−12.3	−7.9
16QAM	Filter 1	−23	−23
	Filter 2	−19.4	−13.5
	Filter 3	−19.6	−16.7
	Filter 4	−19	−15
	Filter 5	−20.3	−18.7
	Filter 6	−18.4	−14

Table 4.1: QPSK and 16QAM Unweighted Crosstalk levels for a 1 dB OSNR penalty

Table 4.1, shows the unweighted crosstalk level values are taken from figures 4.7 and 4.8, for a 1 dB OSNR penalty. We analyse the unweighted crosstalk levels for each filter and WSS type in both QSPK and 16QAM MCSs. As predicted before, we can confirm in terms of filter performances that filter 6 is the one with the best performance regarding the OSNR penalty. Filter 5 presents the worst performance if we ignore filter 1.
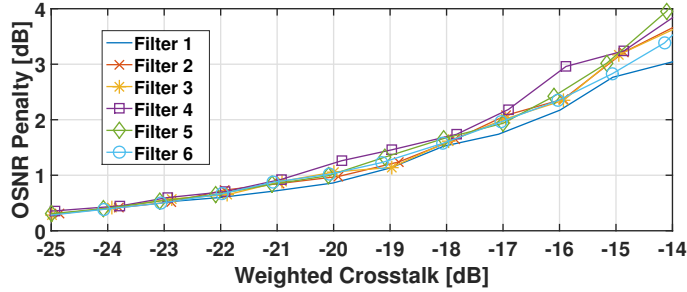
(a)
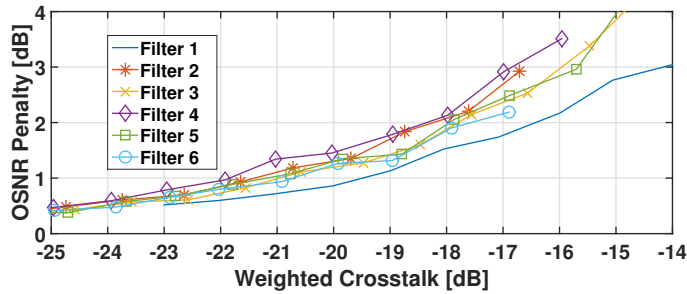
(b)

Figure 4.9: OSNR penalty with QPSK vs weighted crosstalk for $BER = 10^{-3}$ with −5 dB filter (a) and −10 dB filter (b).

Figures 4.9 and 4.10 show the OSNR penalty as a function of the weighted crosstalk power ratio with QPSK and 16QAM modulations, respectively, for each filter type.

By looking at figures 4.9 and 4.10, we can see that regardless of the filter shape used, the OSNR penalty curves have very similar behaviors.
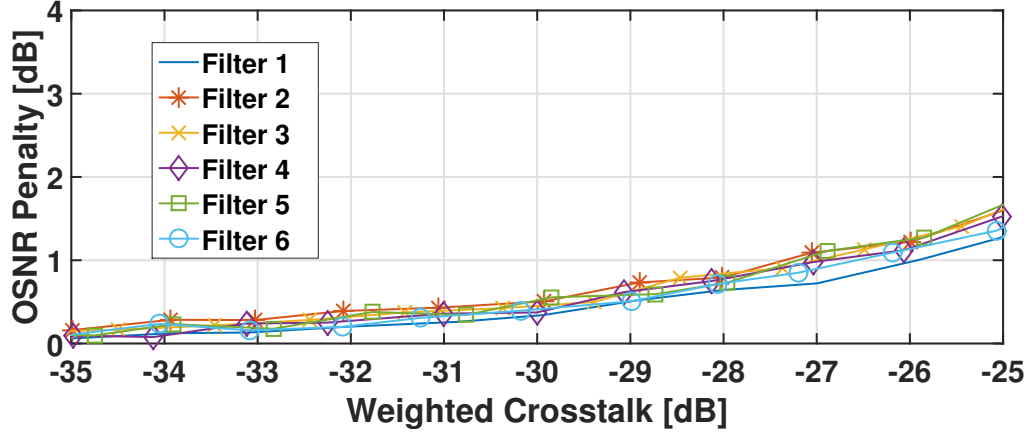
(a)
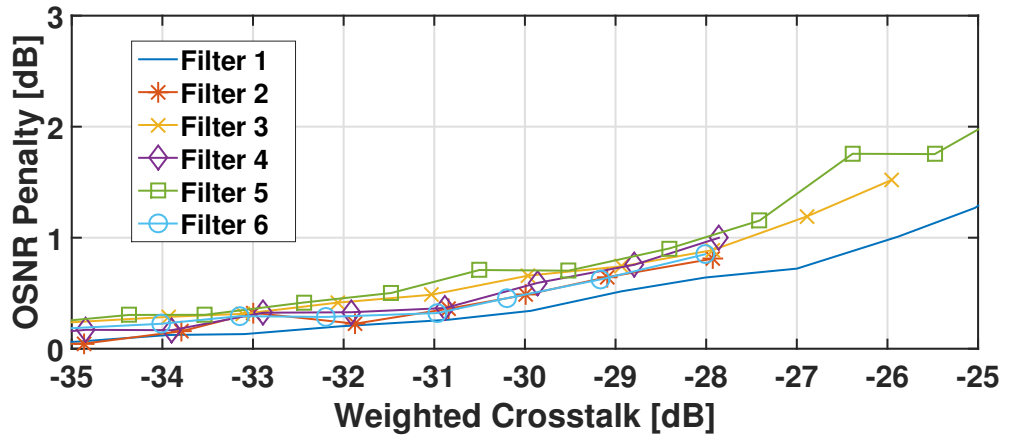
(b)

Figure 4.10: OSNR penalty with 16QAM vs weighted crosstalk for $BER = 10^{-3}$ with -5 dB filter (a) and -10 dB filter (b).

Table 4.2 shows the weighted crosstalk levels obtained for a 1 dB OSNR penalty for both QPSK and 16QAM MCSs, as well as for the different filter types. In table 4.2, all filters lead roughly to similar OSNR penalties, especially for the filters with -5 dB amplitude in the rejection bandwidth.

Weighted Crosstalk			
Modulation	WSS Filter	WSS Type	
		−5 dB	−10 dB
QPSK	Filter 1	−19.5	−19.5
	Filter 2	−19.9	−21.5
	Filter 3	−20	−21
	Filter 4	−20.7	−21.9
	Filter 5	−20	−21
	Filter 6	−20	−20.7
16QAM	Filter 1	−26	−26
	Filter 2	−27.4	−27
	Filter 3	−27	−27.6
	Filter 4	−27	−27.9
	Filter 5	−27.3	−28
	Filter 6	−26.6	−27.5

Table 4.2: QPSK and 16QAM Weighted Crosstalk levels for a 1 dB OSNR penalty.

For -10 dB amplitude, the OSNR penalty variation range is at most 2.3 dB, between filter 1 and filter 4. Like we mentioned earlier, the way these curves are obtained is prone to introduce small variations, but comparing weighted vs unweighted crosstalk results it is clear that the weighted crosstalk curves are much closer to being overlaped. This happens because when we calculate the OSNR penalty due to weighted crosstalk, the effects of the spectral shape of the interfering signal are taken into account. Essentially, the advantage of using the weighted crosstalk metric is to be able to predict OSNR penalties independently of the blocking filter shape [20]. Such is not possible with the unweighted crosstalk metric.

4.6 Conclusions

In this chapter, we described and validated the crosstalk model used in the MC simulator. The validation was done by comparing the OSNR penalties obtained in our studies with the results exhibited in [4], and a good agreement has been reached.

The OSNR degradation caused by in-band crosstalk signals in a coherent receiver, with different modulations schemes, different WSS types and different crosstalk metrics, was studied and evaluated through DEC.

Two different types of crosstalk metrics were studied, unweighted crosstalk and weighted crosstalk. Using QPSK and 16QAM, it was observed that by measuring the OSNR penalty with unweighted crosstalk metric, the type of filter used heavily influences the OSNR penalty. A WSS with blocking filters that block the center bandwidth, where the majority of the channel power lies, showcased less signal degradation caused by crosstalk signals. WSSs with blocking filters that have smaller blocking bandwidths exhibited the worst performance degradations, since the crosstalk signals are not blocked in a significant matter.

Evaluating the same cases with the weighted crosstalk metric, it was observed that regardless of what type of WSS used in the MC simulation, the OSNR penalties were closer than before.

This means that all the different WSS exhibited similar system performances when measured with the weighted crosstalk metric. For both modulation schemes, we conclude that weighted crosstalk allows us to predict system performance regardless of the type of filter being used in the WSS. In addittion, we can extend this technique to scenarios with multiple crosstalk sources such as multidegree ROADM networks [9].

Chapter 5

Conclusions and Future Work

The main conclusions of the developed work in this dissertation are presented in this chapter, as well as suggestions for future work.

5.1   Final Conclusions

In this master thesis, the performance of a M-QAM coherent receiver in presence of in-band crosstalk in an optical network with ROADM nodes, has been investigated using unweighted and weighted crosstalk metrics.

In chapter 2, we studied the coherent receiver as well as some of its components and its model. We also mathematically analyzed the coherent detected signal in the presence of ASE noise and we presented the method DEC, used in this work to evaluate the performance of the coherent receiver. Lastly, we described the MC simulator, which was developed to assess the performance of the coherent receiver.

Chapter 3 was devoted to the study of ROADMs. Several ROADM components were described, given emphazis on one particular component, the WSS. It was studied how this component plays a significant role, in both two-degree and multi-degree ROADM nodes, moving from fixed add/drop to colorless add/drop structures. We also described how WSS brought several advantages to add/drop structures of ROADM nodes, making possible ROADM node implementations with colorless, directionless and contentionless features. ROADM nodes with these features bring a more dynamic and efficient wavelength assignment at the node level, which translates in a decrease of the wavelength congestion at network level.

To complete this chapter, two different node architectures or routing strategies were studied: Route-and-Select and Broadcast-and-Select. In each node, the desired wavelengths at the node input are routed to the selected output ports in the first architecture, while on the second architecture, all input wavelengths are routed to all output ports. B&S is more advantageous in scenarios without crosstalk and with 9 or less port counts, having lower overall system penalties than R&S in these test cases. For higher port counts, R&S was considered the best node architecture to use, especially in the presence of crosstalk.

In Chapter 4, we studied the impact of the in-band crosstalk on the QPSK and 16-QAM coherent receiver performance. The MC simulation model validation, through comparison of its performance estimates with the results found in [4] was presented. This validation was done using unweighted crosstalk metric, but in this work an additional crosstalk metric was studied, weighted crosstalk, and its mathematical expressions presented.

We proceeded to study the coherent receiver performance degradation caused by in-band crosstalk, with both unweighted and weighted crosstalk metrics. In order to do so, several WSSs were used in the MC simulation and each WSS had a different optical filter profile. For both QPSK and 16QAM and using the unweighted crosstalk metric, it was observed that WSSs which had a filter with a wider rejection bandwidth in the center of the optical channel, had lower OSNR penalties due to crosstalk signals. However, using the weighted crosstalk metric, all different WSSs presented similar performances regarding OSNR penalty. This is explained by the fact that weighted crosstalk metric takes into account that spectral content closer to the center of the channel bandwidth, has more impact than spectral content which is closer to the edges of the channel bandwidth. What was observed for both modulation formats, is that the weighted crosstalk metric allows us to predict system performance regardless of the filter shape present in the WSS. Another advantage of weighted crosstalk metric, is that this technique can be extended to scenarios with multiple crosstalk sources, such as multi-degree ROADM networks [20].

5.2 Future Work

We propose the following topics that were not addressed in this work for future investigation:

- Analysis of the impact of multiple interfering terms on the performance of the M-QAM coherent receiver with weighted crosstalk metric, while using a single multi-degree ROADM node,

- While considering crosstalk constraints, study of the impact of several ROADM nodes (two-degree and multi-degree ROADM nodes) on the performance of the M-QAM coherent receiver with weighted crosstalk metric.

- Study of the performance impact on the M-QAM coherent receiver with weighted crosstalk metric using two different node architectures: broadcast-and-select and route-and-select, both in an optical network with multi-degree ROADM nodes and considering crosstalk constraints.

Bibliography

[1] M. Seimetz, *"High-Order Modulations for Optical Fiber Transmission"*, Atlanta, GA: Springer, 2009.

[2] I. Monroy and E. Tangdiongga, *"Crosstalk in WDM Communication Networks"*, Norwell, MA: Springer, 2002.

[3] M. Filer and S. Tibuleac, *"Generalized weighted crosstalk for DWDM systems with cascaded wavelength-selective switches"*, Research and Development Optical Systems, ADVA Optical Networking, 5755 Peachtree Industrial Blvd, Norcross, Georgia 30092, USA 2012.

[4] P. J. Winzer, A. H. Gnauck, A. Knoczykowska, F. Jorge, and J.-Y. Dupuy, *"Penalties from In-Band Crosstalk for Advanced Optical Modulation Formats"*, in 37th European Conference and Exhibition on Optical Communication (ECOC), Sep. 2011, paper Tu.5.B.7.

[5] P. Winzer, S. Chandrasekhar and X. Liu, *"Modulation Formats and Receiver Concepts for Optical Transmission Systems"*. Short course at OFC/NFOEC 2012.

[6] R. Essiambre, G. Kramer, P. Winzer, G. Foschini and B. Goebel, *"Capacity Limits of Optical Fiber Networks"*. J. Lightw. Technol., vol. 30, no 24, pp. 662-701, Feb. 15 2010.

[7] X. Liu and M. Nazarathi, *"Coherent, Self-coherent and Differential Detection Systems"*. Book Chapter, Impact of Nonlinearities on Fiber Optic Communications, S. Kumar, Berlin: Germany, Springer Verlag, 2011.

[8] J. Homa and K. Bala, *"ROADM Architectures and their Enabling WSS technology"*. IEEE Comm. Magazine, Jun. 2008.

[9] S. Tibuleac and M. Filer, *"Trends in Next-Generation ROADM Networks"*, in Proc. ECOC 2011, paper Th.12.A.1, 2011.

[10] W. Way, *"Next Generation ROADM Architectures"*, in Proc. ACP 2012, paper AS1G.3, 2012.

[11] S. Tibuleac, and M. Filer, *"Transmission Impairments in DWDM Networks with Reconfigurable Optical Add-Drop Multiplexers"*, J. Lightw. Technol., vol. 28, no 4, pp. 557-568, Feb. 15, 2010.

[12] S. Gringeri et al, *"Flexible Architectures for optical Transport Nodes and Networks"*, IEEE Comm. Magazine, pp. 40-50, Jul. 2010.

[13] T. Strasser and J. Wagener, *"Wavelength-Selective Switches for ROADM Applications"*, IEEE J. of Selected Topics in Quantum Electronics, vol.16, no 5, pp. 1150-1157, Sep. 2010.

[14] A. Cartaxo, *"Representation of Bandpass Signals and Systems"*, apontamentos de disciplina IST.

[15] M. Jeruchim, P. Balaban, K. Shanmugan, *"Simulation of Communication Systems – Modeling, Methodology, and Techniques."* Berlin: Germany, Springer Verlag, 2009.

[16] A. B. Carlson, P. B. Crilly, *"Communication Systems - An Introduction to Signals and Noise in Electrical Communication."* McGraw-Hill Science/Engineering/Math; 5th edition, Feb. 25, 2009

[17] G. J. F. Martins, *"Monte-Carlo Simulation of an Optical Differential Phase-Shift Keying Communication System with Direct Detection Impaired by In-Band Crosstalk"*, Dissertation presented in partial fulfillment of the Requirements for the Masters Degree on Telecommunications and Information Science, ISCTE-IUL, 2012

[18] B. R. P. Pinheiro, *"Impact of In-Band Crosstalk on the Performance of Optical Coherent Detection Communication Systems"*, Dissertation presented for the Masters Degree on Telecommunications and Information Science, ISCTE-IUL, 2015

[19] M. Filer, S. Tibuleac, ADVA Optical Networking, Norcross GA *"Performance Tradeoffs of 120 GB/s DP-QPSK in ROADM Systems Employing Broadcast-and-Select Versus Route-and-Select Architectures"*

[20] Y. Hsueh, A. Stark, C. Liu, T. Detwiler, S. Tibuleac, M. Filer, Gee-Kung and S. E. Ralph *"Passband Narrowing and Crosstalk Impairments in ROADM-Enabled 100G DWDM Networks."* Journal of Lightwave Technology, vol. 30, no. 24, Dec. 15, 2012

[21] X. Liu and M. Nazarathy, "Coherent, Self-Coherent and Differential Detection Systems" in *"Impact of Nonlinearities on Fiber Optic Communications"*, New York, Ny: Springer, 2011, vol. 7, ch. 1, pp. 1-42.

[22] L. Binh, *"Digital Processing: Optical Transmission and Coherent Receiving Techniques"*, CRC Press, 2014

[23] G. Agrawa, *"Fiber-Optic Communication Systems"*, 4th ed, John Wiley and Sons, 2010.

[24] J. Proakis and M. Salehi, *"Digital Communications"*, 5th ed., McGraw-Hill, 2008.

[25] A. Carlson and P. Crilly, *"Communication Systems"*, 5th ed., McGraw-Hill Education, 2010.

[26] R. Hui and M. O'Sullivan, *"Fiber Optic Measurement Techniques"*, Elsevier Academic Press, 2008.